

1 **α -Catenin stabilises Cadherin-Catenin complexes and modulates actomyosin dynamics to**
2 **allow pulsatile apical contraction.**

3
4 Jaime Jurado¹, Joaquín de Navascués² and Nicole Gorfinkiel¹

5
6 ¹Centro de Biología Molecular “Severo Ochoa”, CSIC-UAM, Cantoblanco, Madrid, Spain.

7 ²European Cancer Stem Cell Research Institute, School of Biosciences, Cardiff University, Cardiff
8 CF24 4HQ, UK.

9 *Author for correspondence (email: ngorfinkiel@cbm.csic.es)

10
11 Abstract:

12
13 We have investigated how cell contractility and adhesion are functionally integrated during
14 epithelial morphogenesis. To this end, we have analysed the role of α -Catenin, a key molecule
15 linking E-Cadherin-based adhesion and the actomyosin cytoskeleton, during *Drosophila* embryonic
16 dorsal closure, by studying a newly developed allelic series. We find that α -Catenin regulates
17 pulsatile apical contraction in the amnioserosa, the main force-generating tissue driving closure of
18 the embryonic epidermis. α -Catenin controls actomyosin dynamics by stabilising and promoting
19 the formation of actomyosin foci, and also stabilises DE-Cadherin at the cell membrane, suggesting
20 that medioapical actomyosin contractility regulates junction stability. Furthermore, we uncover a
21 genetic interaction between α -Catenin and Vinculin, and a tension-dependent recruitment of
22 Vinculin to amnioserosa apical cell membranes, suggesting the existence of a mechano-sensitive
23 module operating in this tissue.

24
25
26
27
28 Key words: α -Catenin, DE-Cadherin, oscillations, apical contraction, actomyosin, Vinculin,
29 morphogenesis

1 Introduction

2
3 Epithelial morphogenesis, the coordinated set of cell movements that generates biological shape,
4 requires the integration of the activity of the actomyosin cytoskeleton with cadherin-based
5 junctions, allowing the coordination of local cell shape changes into tissue-level deformations
6 (Heisenberg and Bellaiche, 2013). There is ample evidence that the actomyosin cytoskeleton
7 influences adhesion dynamics, and conversely, that adherens junctions influence the functioning of
8 the contractile machinery, suggesting complex biochemical and mechanical feedback mechanisms
9 that are only starting to be elucidated (Lecuit and Yap, 2015; Yap et al., 2015).

10
11 E-Cadherin-based junctions are fundamental adhesion centres of epithelial cells that are physically
12 linked to the actomyosin cytoskeleton. α -Catenin is a key protein in maintaining this link by
13 binding to E-Cadherin through its interaction with β -catenin and to F-actin, directly, through its C-
14 terminal domain. Although biochemical studies had challenged the notion that the cadherin-catenin
15 complex binds directly to F-actin (Drees et al., 2005; Yamada et al., 2005), recent experimental
16 findings using an optical trap assay show that strong and stable bonds between the cadherin-catenin
17 complex and an actin filament form under force, probably requiring a conformational change of α -
18 Catenin (Buckley et al., 2014). Force-dependent conformational changes in vertebrate α E-Catenin
19 regulate its binding to Vinculin, an actin-binding protein, and reinforce inter-cellular
20 adhesion (Kim et al., 2015; le Duc et al., 2010; Yao et al., 2014; Yonemura et al., 2010). Moreover,
21 using a FRET tension sensor, it has been shown that the actomyosin cytoskeleton exerts tensile
22 forces on E-Cadherin in an α -Catenin dependent manner (Borghini et al., 2012). Altogether, these
23 observations show that α -Catenin is a key mechano-sensory protein transmitting actomyosin
24 cytoskeletal tension to the cell membrane.

25
26 In spite of these observations, how α -Catenin contributes to the dynamic remodelling of cells in the
27 context of tissue morphogenesis has remained less explored. Recently, detailed structure-function
28 analysis of α -Catenin in *Drosophila* has shown that *in vivo*, the persistent physical linkage between
29 the Cadherin-Catenin complex and the actin cytoskeleton is absolutely required for α -Catenin
30 function (Desai et al., 2013). α -Catenin can bind to actin through its C-terminal actin-binding
31 domain. For example, in the actin-binding domain of *C. elegans* α -Catenin, discrete regions and
32 specific residues have been shown to modulate attachment to junctional actin during epidermal
33 morphogenesis (Maiden et al., 2013). However, there is also evidence that the interaction of α -
34 Catenin with other actin-binding proteins such as Formin and EPLIN can provide an indirect link to
35 the actin cytoskeleton that is likely to contribute to particular aspects of α -Catenin function during
36 morphogenesis (Huveneers and de Rooij, 2013; Maiden and Hardin, 2011). These results suggest

1 complex interactions between α -Catenin, other actin-binding proteins, and the actomyosin
2 cytoskeleton, during morphogenesis, remaining to be elucidated.

3
4 To have a better understanding of α -Catenin role during morphogenesis, we have analysed its
5 function during Dorsal Closure (DC), a morphogenetic process that is being widely used as a
6 model system to understand the interplay between cell activity and mechanics (Gorfinkiel et al.,
7 2011). After germband retraction, the dorsal side of the *Drosophila* embryo is covered by an extra-
8 embryonic epithelium, the amnioserosa (AS). During DC, the AS contracts through the apical
9 contraction of its individual cells, and the lateral epidermis converges towards the dorsal midline,
10 to eventually generate epidermal continuity (Jacinto et al., 2002; Kiehart et al., 2000). Apical
11 contraction in AS cells is pulsatile, driven by periodic contractions of the actomyosin cytoskeleton
12 at the apical surface of cells (Blanchard et al., 2009; David et al., 2013; Martin et al., 2009; Solon
13 et al., 2009). The mechanism underlying the emergence of this oscillatory activity and how it is
14 stabilised to give rise to effective cell shape changes has been a matter of intense research during
15 the last years (Gorfinkiel, 2016). Several studies have revealed that the control of Myosin
16 phosphorylation is fundamental for the appearance of actomyosin oscillations and for its proper
17 dynamics (Munjal et al., 2015; Vasquez et al., 2014). In contrast, the contribution of adhesion to
18 pulsatile actomyosin activity has been less explored even though the engagement of the medial
19 actomyosin cytoskeleton to the membrane is fundamental for cell shape changes to occur. While it
20 has been proposed that apical contraction is triggered by the engagement of a link between cell-cell
21 junctions and an intrinsically contractile actomyosin network (Roh-Johnson et al., 2012), the
22 molecular basis of this link remains unknown. Thus, investigating the nature and dynamics of the
23 link between the actomyosin cytoskeleton and the cell membrane is essential to understand the
24 mechanisms driving apical contraction.

25
26 We have generated an allelic series for α -Catenin and investigated the requirements for α -Catenin
27 during *Drosophila* DC, and in particular, in the contraction of the AS. We show that α -Catenin is
28 required for the dynamics of actomyosin activity and the stabilisation of E-Cadherin at the cell
29 membranes. Furthermore, we find that Vinculin has both α -Catenin-dependent and independent
30 functions, and that Vinculin is recruited to the apical cell membrane of AS cells in a Myosin-II-
31 dependent manner. Altogether, our results suggest that both α -Catenin and Vinculin are part of a
32 mechano-sensitive module operating in AS cells.

33 34 35 **Results**

1 Mutations in the actin-binding domain of α -Catenin are loss of function alleles.

2 α -Catenin is a multi-domain protein composed of three main functional modules: (i) an N-terminal
3 VH1 domain, containing the Armadillo-binding and the homodimerization domains, (ii) a central
4 region, containing a Vinculin binding site (VBS) and the VH2 domain, which can undergo
5 conformational changes in response to actomyosin-generated tension and, (iii) a C-terminal domain
6 VH3 that binds to F-actin (Fig. 1B). To study α -Catenin function in the context of a developing
7 organism, we carried out a chemical mutagenesis in a background bearing a proximal FRT site (see
8 Materials and Methods) and isolated 4 alleles for α -Catenin (Fig. 1A,B). Although several mutant
9 constructs for *Drosophila* α -Catenin have been generated (Desai et al., 2013), their functional
10 analysis requires them to be over-expressed. Having α -Catenin mutant alleles at the endogenous
11 locus ensures that the expression of the mutant proteins is under normal transcriptional control. A
12 missense mutation was identified in α -Cat¹³, producing a substitution of a conserved Valine for a
13 Methionine at position 851 and thus located in the VH3 actin-binding domain of α -Catenin (Fig.
14 1C). The other three alleles are nonsense mutations that generate a premature stop codon at
15 residues Q459, Q668 and Q700. The latter two (α -Cat²⁰⁴⁹ and α -Cat¹⁸⁸³, respectively) completely
16 delete the actin-binding domain. α -Cat⁴²¹ deletes the actin-binding domain and part of the VH2
17 domain, leaving the VBS unaffected (Fig. 1B). We have focused on the analysis of the α -Cat¹³, α -
18 Cat²⁰⁴⁹ and α -Cat⁴²¹ alleles.

19
20 It has been shown that the VH1 domain is the most important for α -Catenin localization at the cell
21 membrane (Desai et al., 2013). This suggested that the alleles generated in this work would
22 produce mutant proteins that are able to localize at the cell membrane. Since the visualization of
23 the localization of the mutant protein in zygotic mutant embryos is not possible due to the maternal
24 contribution, we tested the sub-cellular localization of the mutant proteins in mitotic recombination
25 clones in wing imaginal discs (Fig. 1D). We observe that the three mutant proteins localize at the
26 membrane in the epithelia of wing imaginal discs and suggest they could interfere with the link of
27 the actomyosin cytoskeleton with the cell membrane.

28
29 Although we could not identify the localization of mutant α -Catenin proteins in the embryos, we
30 analysed whether the levels of full-length α -Catenin were affected in DC zygotic mutant embryos
31 for our mutants α -Cat¹³, α -Cat⁴²¹ and α -Cat²⁰⁴⁹, as well as α -Cat¹, a deficiency removing the first
32 exon of α -Cat that includes the translation start site, and therefore a protein null allele (Sarpal et
33 al., 2012). Immunoblot analysis of stage 13 zygotic mutant embryos (Fig. 1E-G) shows that the
34 levels of the full length-protein are substantially decreased in extracts from α -Cat²⁰⁴⁹ and α -Cat⁴²¹
35 homozygous mutant embryos, significantly more than in embryos mutant for α -Cat¹. These results
36 suggest that in α -Cat²⁰⁴⁹ and α -Cat⁴²¹ mutant embryos, there is a destabilisation of the maternal

1 wild-type protein, and thus may aggravate the phenotype of an α -Catenin null homozygote. The
2 presence and stability of mutant proteins is difficult to assess: α -Cat¹³ will have the same size as
3 wild-type α -Cat; bands at the predicted truncated size for α -Cat²⁰⁴⁹ are present also in the wild-
4 type, α -Cat¹ and α -Cat¹³ lanes. While both α -Cat⁴²¹ and α -Cat²⁰⁴⁹ mutations render their respective
5 mRNAs sensitive to the Nonsense-Mediated Decay pathway-mediated degradation, this should
6 lead to null phenotypic conditions (Frischmeyer and Dietz, 1999). Our results below show that this
7 is not the case, which together with the results from the clonal analysis showing that the mutant
8 proteins localize to the cell membrane, lead us to assume that biologically relevant amounts of
9 truncated α -Cat species are present in α -Cat⁴²¹ and α -Cat²⁰⁴⁹ mutant embryos at the DC stage,
10 however undetected by Western Blotting.

11

12 We thus hypothesized that these different mutant alleles could help us understand the function of
13 α -Catenin during tissue morphogenesis. The cuticle laid by these embryos develops anterior
14 defects indicative of a failure in head involution (Fig. 1H-N), as it has been previously shown for
15 α -Cat¹ (Sarpal et al., 2012). However, we noted that a significant percentage of these embryos also
16 exhibit holes in which the posterior limit of the hole is aligned with the first abdominal segment
17 (Fig. 1J). A small percentage of embryos also developed a complete dorsal open cuticle or dorsal
18 holes (Fig. 1K,L). These phenotypes are indicative of DC defects and suggest that in α -Catenin
19 mutants, both head involution and DC are compromised. DC and head involution are two tightly
20 linked morphogenetic processes, involving some of the same tissues and relying on identical
21 genetic pathways (VanHook and Letsou, 2008), and thus it is not uncommon that both processes
22 are affected.

23

24 Cellular forces and adhesion during DC are disrupted in α -Catenin mutants

25 To better understand why the cuticle defects arise in α -Catenin mutant embryos, we performed
26 time-lapse movies of homozygous mutant embryos for the different α -Catenin alleles carrying an
27 endogenously tagged DE-Cadherin::GFP to visualize cell contours (Fig. 2A; Movie 1, 2). These
28 embryos are able to progress until mid-embryogenesis and to start DC normally due to the maternal
29 contribution of α -Catenin. However, in most of the embryos defects start appearing during DC due
30 to the anterior canthus not forming properly: the dorsal ridge primordia, two contra-lateral
31 epithelial structures that form where the dorsal epidermis abuts the head segments, do not elongate,
32 nor move toward the dorsal midline nor fuse to create the dorsal ridge (Fig. 2Aii,ii'). As a
33 consequence, there is no anterior migration of the dorsal ridge and the head segments are left on the
34 outside instead of moving inside the dorsal anterior epidermis (Fig. 2Aiii,iii'). As DC progresses,
35 the anterior epidermis and the AS tear apart. The dorsal most epidermal cells detach from the AS in
36 a region spanning the anterior half of the AS in several embryos (Fig. 2Aiv,iv'). Meanwhile, the

1 posterior canthus forms and progresses towards the centre of the dorsal midline but tears at the
2 anterior side prevent completion of DC.

3
4 To analyse the evolution of DC quantitatively, we measured the velocity (v) of progression of the
5 leading edge by measuring the width of the AS at its symmetry axis (Fig. 2A). This provides a
6 quantitative way to assess whether the forces contributing to DC are affected (Hutson et al., 2009).
7 We observe that in all the alleles analysed there is a decrease in v (Fig. 2Bii-iv) except for α -Cat^l
8 (Fig. 2Bi), indicating that the point mutations lead to distinct phenotypes. Since some of the
9 embryos analysed have tears at the anterior canthus as described above, we asked whether the
10 reduction in v resulted largely from the anterior tears. It was possible to test for this in α -Cat^l and
11 α -Cat^{42l} mutant embryos, as not all of the individuals analysed showed anterior tears. Interestingly,
12 we observe that the presence of a hole does not affect v in α -Cat^l mutant embryos (Fig. S2Ai-ii).
13 However, even in the absence of anterior tears, there is a reduction in v in α -Cat^{42l} mutant embryos
14 (Fig. S2Aiii-iv), suggesting that cellular forces contributing specifically to DC are defective.

15
16 One of the processes contributing to DC is the apoptosis-mediated extrusion from the plane of the
17 AS epithelium of around 10% of cells (Kiehart et al., 2000), through a mechanism involving
18 cytoskeletal rearrangements in the delaminating cell and also in its nearest neighbours (Meghana et
19 al., 2011; Mulyil et al., 2011). It has been shown that increasing the number of cell delamination
20 events hastens closure (Toyama et al., 2008). Thus, we asked if the decrease in closure velocity
21 could be due to a decrease in cell delamination events. We observe that, while the total number of
22 AS cells at the onset of tissue contraction is similar to the wild-type, the number of cell
23 delamination events increases in α -Catenin mutant embryos (Fig. 2C,D), but not the location or
24 timing of these events (data not shown). Thus, these results show that changes in the delamination
25 rate are not responsible for the decrease in closure velocity.

26
27 These observations suggest that a variety of defects underlie the embryonic phenotype of α -
28 Catenin mutant embryos. Time-lapse movies show that the anterior dorsal ridge is the most
29 affected tissue, disrupting both head involution and DC. The actin purse string is also affected, as
30 shown by a decrease in actin accumulation (Fig. S2B). Finally, the decrease in closure velocity,
31 which cannot be attributed to the anterior holes or to a decrease in cell extrusions, suggests that the
32 contraction of the AS may be affected. We are particularly interested in exploring the contribution
33 of α -Catenin to the emergence of the contractile force of the AS, to understand how actomyosin
34 contractility and adhesion are integrated to give rise to cell and tissue changes in shape.

35
36 Loss of α -Catenin slows down the oscillatory and contractile behaviour of AS cells.

1 To investigate the role of α -Catenin in the contraction of the AS, we quantitatively analysed the
2 oscillatory and contractile behaviour of AS cells during the whole process of DC (Fig. 3; Movie 3).
3 We automatically tracked AS cells from 4-5 embryos for each α -Catenin allele and measured the
4 frequency and amplitude of apical cell shape oscillations as previously described (Blanchard et al.,
5 2010). We have shown that the cycle length and amplitude of apical cell area oscillations shows a
6 temporal pattern over DC. During early stages of DC, AS apical cell area fluctuates with long cycle
7 lengths and high amplitude. The onset of whole tissue contraction coincides with a decrease in both
8 the cycle length and the amplitude of cell oscillations. Sixty minutes into this phase, zippering from
9 the canthi engages, and cells enter a fast mode of oscillations with low amplitude and short cycle
10 length.

11
12 In α -Cat¹³ mutant embryos, the spatiotemporal pattern of the cycle length of apical cell area
13 oscillations is almost identical to the wild-type (Fig. 3B). The amplitude of cell oscillations is only
14 mildly affected in α -Cat²⁰⁴⁹ and not at all in α -Cat⁴²¹ embryos (Fig. 3C). By contrast, there is a
15 clear increase in the period of oscillations in α -Cat²⁰⁴⁹ mutant embryos, for almost two hours of
16 development. α -Cat⁴²¹ embryos display a similar, albeit milder increase in period, mostly at later
17 stages (Fig. 3B). Our previous results have shown that an important signature of the pulsatile
18 contractile behaviour is the ratio of the duration of the expansion half-cycle to the contraction half-
19 cycle, with lower ratios being consistent with a more contracted state (Blanchard et al., 2010).
20 Thus, we analysed whether the duration of the half-cycles was differentially increased in these
21 mutant embryos. We observe an increase in both the contraction and the expansion half-cycles
22 lengths in α -Cat²⁰⁴⁹ and α -Cat⁴²¹ mutants, with the expansion half-cycle being more significant,
23 and over a longer developmental period (Fig. 3D,E). This is also evident in the ratio of the duration
24 of the expansion half-cycle to the contraction half-cycle, which is greater in α -Cat²⁰⁴⁹ and α -Cat⁴²¹
25 but not in α -Cat¹³ mutant embryos (Fig. S3A). Thus, these results suggest that AS cells are not
26 contracting properly in α -Cat²⁰⁴⁹ and α -Cat⁴²¹ mutant embryos. In accordance with this, the rate of
27 apical cell contraction is lower in these embryos (Fig. S3B). Interestingly, we found that AS cells
28 from α -Cat⁴²¹ and α -Cat²⁰⁴⁹ mutant embryos develop a corrugated appearance (Fig. 3Aii', compare
29 with 3Aii), which indicates that the apical cell perimeter is not able to shrink properly. We
30 measured the ratio of apical cell perimeter to apical cell radius and observed a significant increase
31 in this ratio in later stages of DC (Fig. S3C). Altogether, our results show that the apical
32 contraction of these cells is defective.

34 *α -Catenin regulates the dynamics of actomyosin foci*

35 Apical cell oscillations result from Myosin-driven oscillatory contractions of a medial actin
36 network spanning the apical medial region of AS cells (Blanchard et al., 2010; David et al., 2010).

1 Myosin and actin co-localize tightly at the medioapical cortex of AS cells forming transient
2 accumulations or foci, and both Myosin and F-actin reporters can be used to follow their dynamics
3 (Blanchard et al., 2010; David et al., 2010). To elucidate whether the slower oscillatory dynamics
4 in α -Catenin mutants result from perturbed actomyosin activity, we performed time-lapse movies
5 of AS cells carrying the F-actin reporter sGMCA (Movie 4, 5). Then we measured the duration and
6 time interval of F-actin foci over a 15-minute time window, during the slow phase of DC (Fig.
7 4A,B), when oscillation defects are more significant.

8
9 The mean duration of the actin cycle increases in AS cells from α -Cat²⁰⁴⁹ and α -Cat⁴²¹ mutant
10 embryos but not in α -Cat¹³ embryos (Fig. 4C), correlating with the increased period of cell
11 oscillations in the former but not in the latter mutant backgrounds. Interestingly, the time interval
12 between consecutive actin foci increases in the three alleles, but significantly more in α -Cat⁴²¹ and
13 α -Cat²⁰⁴⁹ mutant embryos (Fig. 4D). This suggests that the increase in the expansion half-cycle
14 length in these embryos could be a direct consequence of the increase in the time interval between
15 consecutive foci. In contrast, the duration of actin foci decreases in α -Cat¹³ and α -Cat⁴²¹, but not in
16 α -Cat²⁰⁴⁹ embryos (Fig. 4E). Thus, the observed dynamics of actin foci shows a correlation with
17 the oscillatory behaviour of AS cells: while in α -Cat²⁰⁴⁹ and α -Cat⁴²¹ mutant embryos, the increase
18 in the time interval between consecutive foci gives rise to an increase in the cycle length of cell
19 oscillations, this is not the case in α -Cat¹³ embryos, where the low increase in the time interval
20 between consecutive foci together with the decrease in the duration of actin foci cancel out and
21 give rise to a whole actin cycle length indistinguishable from the wild-type.

22
23 To confirm that this change in actin dynamics is a consequence of a defective link between the
24 cytoskeleton and adherens junctions, we also analysed actin dynamics in DE-Cadherin mutant
25 embryos, which provide a situation where α -Catenin levels are further reduced. The *shg*^{g317} mutant
26 allele codes for a truncated DE-Cadherin protein lacking the Armadillo binding domain (Gorfinkiel
27 and Martínez Arias, 2007), thus preventing the interaction of DE-Cadherin with α -Catenin. This
28 allele has a stronger phenotype than the null allele probably through a dominant-negative effect on
29 the maternal protein (Gorfinkiel and Martínez Arias, 2007; Tepass et al., 1996). Time-lapse
30 imaging of *shg*^{g317} mutant embryos carrying the sGMCA reporter (Movie 6) shows that AS cells
31 form actin foci but these show a significantly shorter duration as well as longer time intervals
32 between consecutive foci, than in wild-type embryos (Fig. 5A-D; Table S1).

33
34 Overall, our results suggest that α -Catenin has a role in stabilising actomyosin foci and in
35 promoting the formation of new foci. Interestingly, α -Catenin also regulates medial actomyosin
36 dynamics and polarity in germ-band cells (Rauzi et al, 2010). The particular dynamics of actin foci

1 observed in the alleles analysed here suggest that the interaction of α -Catenin with actin and other
2 actin-binding proteins may be differentially affected in each specific allele.

4 *ECadherin dynamics at cell-cell junctions in α -Catenin mutants*

5 It is known that α -Catenin is required for adherens junction assembly, function and dynamics
6 (Cavey et al., 2008; Desai et al., 2013; Imamura et al., 1999; Pacquelet and Rorth, 2005; Sarpal et
7 al., 2012; Yonemura et al., 2010). Moreover, it has been shown that the actin-binding domain of α -
8 Catenin, and hence the interaction of α -Catenin with the actin cytoskeleton, promotes the
9 localisation of DE-Cadherin and Armadillo at the apical cell membranes (Desai et al., 2013). We
10 thus analysed whether DE-Cadherin levels were also affected in α -Catenin mutant embryos. We
11 could not detect significant changes in DE-Cadherin levels in α -Catenin zygotic mutant embryos,
12 but did detect changes in DE-Cadherin turnover. FRAP experiments on endogenously-tagged DE-
13 Cadherin::GFP embryos show that there is a significant decrease in the mobile fraction of DE-
14 Cadherin as DC progresses, suggesting that DE-Cadherin is stabilised at cell membranes during
15 late stages of the process (Fig. 5E,F). Similarly, FRAP experiments on an α -Catenin::YFP protein
16 trap that is homozygous viable and localizes normally to the cell membrane, also show a decrease
17 in the mobile fraction of α -Catenin as DC progresses (Fig. 5G). However, in α -Cat²⁰⁴⁹ mutant
18 embryos the decrease in DE-Cadherin mobile fraction as DC progresses does not occur (Fig. 5H).
19 Surprisingly, in α -Cat⁴²¹ mutant embryos, the stabilisation of DE-Cadherin with developmental
20 time is recovered (Fig. 5I). These results show that adhesion dynamics is different in α -Cat²⁰⁴⁹ and
21 α -Cat⁴²¹ mutant backgrounds. Interestingly, truncated forms of α -Catenin that bind constitutively
22 to Vinculin strongly stabilise adherens junctions dynamics (Chen et al., 2015; Yonemura et al.,
23 2010). Since the α -Cat⁴²¹ allele removes not only the actin-binding domain but also part of the
24 VH2 domain, our results raise the possibility that in α -Cat⁴²¹ embryos, constitutive binding of α -
25 Catenin to Vinculin rescue DE-Cadherin dynamics.

27 *Interaction between Vinculin and α -Catenin*

28 In mammalian cells, Myosin II-generated tension induces a conformational change in α -Catenin
29 uncovering a VBS. Vinculin is then recruited to adherens junctions and becomes associated with
30 more actin filaments thus reinforcing cell-cell adhesion (Kim et al., 2015; le Duc et al., 2010; Yao
31 et al., 2014; Yonemura et al., 2010). Thus, we decided to investigate whether Vinculin and α -
32 Catenin also interacted during *Drosophila* embryogenesis. A complete deletion of the Vinculin
33 coding sequence (Δ Vinc) is viable and does not cause any visible phenotype (Klapholz et al.,
34 2015). However, Δ Vinc aggravates the cuticular phenotype of α -Cat mutant embryos in an allele-
35 dependent manner, with a decreasing strength series of α -Cat²⁰⁴⁹ > α -Cat^{I3} > α -Cat^I > α -Cat⁴²¹,

1 with the latter showing only a very weak genetic interaction (Fig. 6A,C). These results indicate that
2 α -Catenin genetically interacts with Vinculin. They further show that although the absence of
3 Vinculin does not affect the viability of *Drosophila* embryos and adults, in some α -Catenin mutant
4 backgrounds its activity is able to partially compensate α -Catenin function. Curiously, the α -Cat⁴²¹
5 allele shows the weakest genetic interaction showing that in this allele Vinculin is not able to
6 partially restore α -Catenin function.

7
8 A possible explanation for these results is that the α -Catenin²⁰⁴⁹ and α -Catenin¹³ mutant proteins
9 expose the VBS and bind to Vinculin, which by its binding to the actin cytoskeleton restores α -
10 Catenin function. This would not happen in the α -Catenin⁴²¹ mutant protein, since the absence of
11 Vinculin does not aggravate the phenotype of this allele. However, this is in sharp contrast with
12 what is known about the molecular interaction between α -Catenin and Vinculin. According to the
13 current paradigm, the α -Cat²⁰⁴⁹ protein, which lacks the actin-binding domain (Fig. 1B), would not
14 be stretched to expose the VBS and therefore would not interact molecularly with Vinculin. On the
15 other hand, the α -Cat⁴²¹ protein, whose truncation removes the putative auto-inhibitory domain
16 (Fig. 1B), would expose the VBS and thus would interact with Vinculin in a constitutive manner.

17
18 To better understand these results, we tested the ability of α -Catenin alleles to interact with the
19 actomyosin cytoskeleton, by ectopically expressing a phosphomimetic form of the Myosin
20 Regulatory Light Chain (spaghetti squash), Sqh^{DD}, in the AS of α -Catenin mutant embryos. We
21 hypothesized that increasing actomyosin contractility in the AS of embryos in which E-Cadherin-
22 mediated adhesion is compromised would lead to stronger and more frequent tears if α -Catenin is
23 indeed able to transmit contractile forces to the cell membranes. We observe that the ectopic
24 expression of sqh^{DD} in the AS aggravates the cuticular defects of α -Cat¹ and α -Cat¹³ embryos, but
25 does not have an effect on the cuticular phenotypes of α -Cat²⁰⁴⁹ and α -Cat⁴²¹ embryos (Fig. 6B,C).
26 These results confirm that neither α -Cat²⁰⁴⁹ nor α -Cat⁴²¹ is able to interact properly with the
27 actomyosin cytoskeleton.

28
29 Thus, an alternative explanation that reconciles our results with what is known about the α -
30 Catenin-Vinculin interaction is that in all but the α -Cat⁴²¹ allele, the presence of Vinculin partially
31 rescues the function of α -Catenin, but this rescue is not dependent on the ability of these proteins to
32 interact at the molecular level. Interestingly, an α -Catenin -independent binding of Vinculin to E-
33 Cadherin has been observed in cancer cells devoid of α -Catenin (Hazan et al., 1997). In contrast, in
34 the α -Cat⁴²¹ allele, this function of Vinculin would be prevented because most Vinculin would be
35 bound to α -Catenin in a constitutive manner.

1
2 These results led us to analyse Vinculin localisation in the AS of DC embryos. Recently, a genomic
3 construct containing Vinculin::GFP has been generated, providing a reporter with physiological
4 expression levels (Klapholz et al., 2015). Vinculin::GFP can be seen localising at the apical side of
5 epidermal cells, but in AS cells from early DC embryos fluorescence levels are very low. We
6 observed a small but consistent increase of Vinculin::GFP at the level of the cell membranes in late
7 DC embryos compared to early stages of the process (Fig. 6D), when cells contract faster. We
8 further analysed whether this Vinculin localisation was tension-dependent. We observed an
9 increase of Vinculin levels in early DC embryos when Myosin activity is elevated in the AS
10 through the ectopic expression of a constitutive active form of Myosin Light Chain Kinase (Fig.
11 6E). Similar results were observed with a UAS-Vinculin::YFP reporter expressed in the AS:
12 Vinculin localisation at the apical membrane of AS cells increases as DC progresses (Fig. S4A),
13 and this localisation increases and decreases when constitutive active forms of Myosin Light Chain
14 Kinase and Myosin phosphatase, respectively, are ectopically expressed (Fig. S4B,C).

15
16 Finally, we analysed the localisation of the Vinculin reporter in α -Cat²⁰⁴⁹ and α -Cat⁴²¹ mutant
17 backgrounds. We find that in both mutant backgrounds, Vinculin localises to apical cell
18 membranes (Fig. 6F) and these levels are increased in later embryos compared to the wild-type. We
19 hypothesize that in α -Cat²⁰⁴⁹, Vinculin localises at cell-cell junctions independent of α -Catenin,
20 while in α -Cat⁴²¹, Vinculin localises at cell-cell junctions through direct binding with α -Catenin.

21
22 Altogether, our results suggest that there is a tension-dependent recruitment of Vinculin to the
23 apical membranes of AS cells. Moreover, the observed interactions between α -Catenin and
24 Vinculin suggest both α -Catenin-dependent and α -Catenin-independent roles for Vinculin during
25 *Drosophila* embryogenesis.

26 27 **Discussion**

28
29 How adhesion and actomyosin contractility are integrated at junctions is a fundamental question in
30 morphogenesis. To tackle this we have analysed the role of α -Catenin, a key protein linking
31 adherens junctions and the actin cytoskeleton, in the context of *Drosophila* embryogenesis and in
32 particular during DC. We find that α -Catenin regulates pulsatile actomyosin dynamics in apically
33 contracting cells by stabilising and promoting actomyosin contractions. α -Catenin also stabilises
34 DE-Cadherin at the cell membrane, suggesting that medioapical actomyosin contractility regulates
35 junction stability. Furthermore, our results reveal an interaction between α -Catenin and Vinculin
36 that could be important for DE-Cadherin stabilisation.

1
2 Our live imaging of mutant embryos shows a strong requirement for α -Catenin in the migration of
3 the dorsal ridge primordia towards the dorsal midline, preventing the formation of the dorsal ridge
4 and thus affecting both DC and head involution. These results reveal that the dorsal ridge is
5 particularly sensitive to the levels of α -Catenin and suggest it is a key region that could
6 mechanically coordinate both processes. Although it is clear that some of the defects we observe
7 during DC are a consequence of the defective dorsal ridge morphogenesis, our analysis shows that
8 other cellular processes more specific to DC are affected. In particular, we observe that the actin
9 cable is disorganized and that the pulsatile apical contraction of the AS is abnormal.

10 The defects observed at the level of AS apical cell oscillations could be a consequence of a
11 defective actin cable, which would be acting as a ratchet and thus progressively restricting the
12 expansion of apical cell area (Solon et al., 2009). However, several lines of evidence suggest that a
13 ratchet mechanism stabilising the contracted state of AS cells is acting at the level of individual
14 cells (Blanchard et al., 2010; Wang et al., 2012; Wells et al., 2014). In particular, the analysis
15 performed here of actin oscillatory dynamics in *α -Catenin* mutants suggests that the increase in the
16 expansion half-cycle of AS apical cell oscillations could be due to an increase in the time interval
17 between consecutive foci. Thus, our results favour the idea that the Cadherin-Catenin complex has
18 a role in promoting actomyosin oscillatory dynamics. How α -Catenin promotes actomyosin
19 contractility remains to be elucidated but it is likely to involve both direct and indirect –through
20 other actin-binding proteins– interactions with the actin cytoskeleton. For example, an antagonistic
21 interaction between α -Catenin and the Arp2/3 complex has been observed both in cell systems and
22 in *Drosophila* embryos (Benjamin et al., 2010; Sarpal et al., 2012), raising the possibility that the
23 actin bundling activity of α -Catenin at adherens junctions, rather than the formation of Arp2/3-
24 dependent networks, could be important for apical contraction.

25

26 Interestingly, we find that in the *α -Cat²⁰⁴⁹* allele, adhesion dynamics is also defective, suggesting
27 that medioapical actomyosin dynamics promotes adherens junction stabilisation. In contrast, in the
28 *α -Cat⁴²¹* allele, which would bind constitutively to Vinculin in a context of defective medioapical
29 actomyosin dynamics, DE-Cadherin stabilisation is recovered. This result suggests that the
30 stabilisation of DE-Cadherin could be mediated by the binding of Vinculin to α -Catenin. This is in
31 agreement with what has been observed in cell systems, where forms of α -Catenin that
32 constitutively bind to Vinculin have decreased mobility (Cheng et al., 2015; Yonemura et al.,
33 2010). We further show that although DE-Cadherin is stabilised in *α -Cat⁴²¹* mutants, possibly due
34 to the Vinculin/ α -Catenin interaction, this stabilisation is not able to rescue normal medioapical
35 actin dynamics. Thus, we suggest that α -Catenin direct binding to actin via its actin-binding
36 domain promotes the formation of medioapical actomyosin foci, while indirect binding to actin via

1 Vinculin would promote junction stabilisation. Altogether, our data suggest that α -Catenin
2 domains, through their interactions with other actin-binding proteins and actin, may differentially
3 regulate actin dynamics.

4
5 Finally, our results show that there is a tension-dependent recruitment of Vinculin at the
6 membranes of AS cells, which could be mediated by α -Catenin. Interestingly, it has recently been
7 found using a heat-shock inducible Vinculin reporter, that the rate of change of Vinculin levels
8 correlates with junctional tension (Hara et al., 2016). Our results also suggest that Vinculin is able
9 to perform an adhesive function when α -Catenin function is compromised. This could result from
10 an α -Catenin -independent binding of Vinculin to E-Cadherin (Hazan et al., 1997) or from an
11 interaction between Vinculin and other junctional proteins such as ZO-1, which has been shown to
12 recruit Vinculin to VE-cadherin junctions and increase cell-cell tension (Tornavaca et al., 2015).
13 However, since ZO-1 can also interact with α -Catenin, it remains to be investigated whether the
14 mechano-sensitivity of Vinculin is completely dependent on α -Catenin. Thus, it is likely that
15 Vinculin is able to perform different functions depending on its developmental context.
16 Interestingly, different mechanisms for Vinculin-binding to Talin in integrin-mediated adhesion
17 have recently been uncovered in different morphogenetic processes, allowing Talin to sense
18 different force vectors (Klapholz et al., 2015). Since a role for Talin and integrin-mediated
19 adhesion during DC has been uncovered (Ellis et al., 2013; Narasimha and Brown, 2004; Reed et
20 al., 2004), it would be interesting to investigate whether Vinculin is also involved in integrin-
21 mediated adhesion at this stage. Our results suggest that a tension-dependent module involving
22 Vinculin is present in AS cells. An exciting avenue will be to identify the mechanisms and function
23 of such module in the context of morphogenesis.

24 25 26 **Materials and methods**

27
28 Fly stocks and genetics: The stocks used in this work are listed in Table S2.

29
30 Mutagenesis: Mutagenesis was performed on a *w*; *PBac{WH}ND-MLRQ^{f00651}* background,
31 isogenic for the 3rd chromosome. *PBac{WH}f00651* is inserted at position 23,339,695 of release
32 r6.09 of the *Drosophila melanogaster* genome (estimated cytological band 80E1), approximately
33 2kb proximal to the transcriptional start site of α -Cat. It contains a long FRT sequence to allow for
34 the generation of molecularly defined deletions (Thibault et al., 2004), which makes it also apt for
35 mitotic recombination-mediated clonal analysis (see Fig. 1D). This background was selected
36 because the α -Cat locus is proximal to both FRT80B and FRT2A. While the *PBac{WH}f00651*

1 insertion probably disrupts *ND-MLRQ* function, we found it to be homozygous viable, if fertility is
2 somewhat reduced. For simplicity we renamed this strain as *w;*; *FRT80E1*. We treated 2-3 days
3 old, pre-starved (8 hours), *w;*; *FRT80E1* males with ~0.3% ethyl methanesulfonate in 1% sucrose
4 for 24h, and crossed them to *w;*; *MKRS/TM6B* virgin females. Approximately 4,000 males from the
5 offspring were crossed individually to *α-Cat*^{L004411}/*TM6B* virgin females. *α-Cat*^{L004411} originates
6 from a lethal *PBac{SAstopDsRed}* insertion (Schuldiner et al., 2008) and is a probable
7 transcriptional null. Offspring was tested for complementation of lethality. These lines were re-
8 tested with a custom deficiency between the FRT-bearing insertions *P{RS3}CB-6208-3* (Ryder et
9 al., 2004), located at 23,339,498 (r6.09) (our results), and *PBac{WH}ND-MLRQ*⁰⁵⁹⁶⁶ (Thibault et
10 al., 2004), located at 22,998,301 (r6.09) (Ryder et al., 2004) and our results). This deficiency
11 uncovers the whole *α-Cat* locus as well as other genes and is strongly *Minute*.

12

13 Construction of transgenic line: For the UAS-Vinculin::Venus construct, the cDNA was amplified
14 by PCR, cloned into the entry vector pENTR/D-TOPO by directional TOPO cloning (Gateway
15 System, Invitrogen) and introduced by recombination into the destination vector pTWV (pUAST-
16 Venus).

17

18 Live-Imaging: Stage 12-13 *Drosophila* embryos were dechorionated, mounted in coverslips with
19 the dorsal side glued to the glass and covered with Voltaef oil 10S (Attachem). The AS was
20 imaged at 25-28°C. using an inverted LSM 710 Meta laser scanning microscope with a 40X or a
21 63X oil immersion Plan-Fluor objective. For whole AS imaging, 15-16 z sections 1.5µm apart
22 were collected every 30 seconds. For cytoskeletal dynamics imaging, 5-6 z sections 1µm apart
23 were collected every 15 seconds.

24

25 FRAP experiments: FRAP was performed using an LSM710 laser scanning microscope with a 63X
26 oil immersion Plan-Apochromat (NA=1.4) objective. A circular region of interest (ROI)
27 ($r=0.52\mu\text{m}$) was bleached with a 488nm laser beam at 100% power. Images were taken before and
28 after bleaching every 2s for 2 minutes. A $3.2 \times 3.2\mu\text{m}$ reference region was also imaged to take into
29 account photobleaching effects. For FRAP analysis, normalized fluorescence over time for each
30 individual experiment was fitted to a simple exponential function of the form: $I(t) = A(1-\exp(-bt))$
31 using the MATLAB built-in function `nlinfit` and `nlparci` (MathWorks, Natick, MA), where A is the
32 mobile fraction and b is $\frac{\ln 2}{\tau_{1/2}}$, where $\tau_{1/2}$ is the half time of the recovery. Mean parameters were
33 calculated for each genotype. To assess the significance of differences between early and fast
34 embryos in each genotype we applied a two sample t-test (Statistics toolbox of MATLAB).

35

36 Image analysis: 4-5 embryos for each *α-Cat* allele were used for the morphometric analysis of AS

1 cells. Embryos analysed were not selected on the basis of their gross phenotype and are
2 representative of all the embryos that were imaged. (All embryos imaged and analysed had anterior
3 detachments of varying gravity, except in the case of the α -Cat⁴²¹ allele, for which embryos with
4 and without anterior detachments were analysed but no differences in the parameters analysed were
5 observed between the two classes). Automated tracking of the AS cell shapes was done with
6 custom software written in Interactive Data Language (IDL, Exelis) as described previously
7 (Blanchard et al., 2009; Blanchard et al., 2010). Cell shape fluctuations were analysed as described
8 in (Blanchard et al., 2010). Individual embryos were staged according to three parameters, which
9 have been shown to evolve stereotypically through the course of dorsal closure (Gorfinkiel et al.,
10 2009): cell area, cell shape anisotropy and mediolateral cell length (Fig. S1). This allowed us to
11 determine their developmental time with an accuracy of 10 min. Inter-genotype aligning was done
12 by aligning the tissue strain rate, which in the case of α -Catenin mutant embryos may
13 underestimate possible delays in the onset of net tissue contraction.

14 Actin foci dynamics was computed manually from time-lapses with 15s-time interval, which
15 allowed us to follow the assembly and disassembly of each focus in an accurate manner. Central
16 cells of the AS were chosen to quantify actin dynamics. The times associated with the duration of
17 foci were obtained by counting the number of frames since an actin focus was visible until its
18 signal was lost. The times associated with the time interval between consecutive foci were obtained
19 by counting the number of frames in which no apicomedial actin signal was detected.

20
21 Statistics: Statistical analysis of embryonic cuticles was done using a two-tailed Z-test, which
22 evaluates the significance of the difference of the z-ratio between two independent proportions.
23 Each proportion is calculated by dividing the number of observations within each phenotypic
24 category by the total number of observations. Each allele was compared to the null allele \square -Cat^l. A
25 z-ratio greater than 1.64, 2.33 or 3.09 corresponds to a P-value <0.05, <0.01 or <0.001, respectively.
26 Statistical analysis of actin foci dynamics was done considering each focus as an individual event,
27 computing the duration and time interval of each focus individually. Pooled data of these variables
28 was then compared between genotypes using a Mann-Whitney U-test since they did not follow a
29 standard normal distribution, previously tested with a one-sample Kolmogorov Smirnov test
30 (Statistics ToolBox of MATLAB). Statistical analysis of cell oscillations and other cell parameters
31 was done using a mixed-effect model as in (Butler et al., 2009; Fischer et al., 2014). We estimated
32 the P-value associated with a fixed effect of differences between genotypes, allowing for random
33 effects contributed by differences between embryos within a given genotype, calculated at each
34 time point. Ribbons were drawn for the whole span of analysis for wild-type embryos and for
35 mutant embryos. The mean trends and ribbon width are calculated from data averaged to reduce
36 noise (a box average of eight bins along the abscissa was used). The widths of ribbons straddling
37 mean trends represent a standard error calculated from the sums of within-experiment variance and

1 between experiments variance. To test where mutant embryos were significantly different ($P <$
2 0.05) from wild-type, mixed-model was applied, with embryo as the random variable. The regions
3 where $P < 0.05$ are depicted with a grey-shaded box.

4
5 Immunostainings: Embryos were fixed and stained as previously described (Kaltschmidt et al.,
6 2002). Primary antibody was rat monoclonal against α -Catenin (DCAT-1, 1/20, Developmental
7 Studies Hybridoma Bank, University of Iowa, developed by T. Uemura). Alexa 555 (1/500,
8 ThermoFischer) was used as secondary antibody. DAPI (1/200, Merck) was used for imaginal discs
9 stainings. For actin staining, Phalloidin-TRITC (P-1951, 1/500, Sigma) was added to the PFA (8%
10 solution, EM grade, Electron Microscopy Sciences) and ethanol 80% was used instead of methanol
11 100%. F-actin fluorescence was quantified using ImageJ.

12
13 Immunoblotting: Stage 13 dechorionated embryos were homogenized in SDS sample buffer (62.5
14 mM Tris-HCl pH 6.8, 2.3% SDS, 10% glycerol, 5% β -mercaptoethanol and 0.005% bromphenol
15 blue). Proteins resolved by SDS-PAGE were transferred into nitrocellulose membranes
16 (Amersham). Membranes were blocked in PBS containing 5% milk powder and 0.05% Tween-20
17 for 1 h at 25°C, incubated overnight with primary antibodies at 4°C and then with an HRP-
18 conjugated secondary antibody for 1 h at room temperature. After extensive washes in PBS 0.05%
19 Tween-20, bands were visualized using the ECL system (Biosciences). The following primary
20 antibodies were used: anti- α -Catenin (rat monoclonal DCAT-1, 1/400, DSHB) and anti- β -tubulin
21 (mouse monoclonal E7, 1:1,000; DSHB). HRP-coupled secondary antibodies (Jackson
22 Immunoresearch) were used at 1:1,000.

23 Cuticle preparations: Embryos were collected from 24-hour-old eggs and then aged 48 hours at
24 25°C. They were dechorionated in bleach and mounted with the vitelline membrane in acetic acid-
25 Hoyers (1:1) and the slide was incubated overnight at 65°C.

26 27 **Acknowledgements**

28
29 We are very grateful to Guy B. Blanchard for the development of “oTracks” software and for
30 discussions and to Alfonso Martinez Arias, in whose lab the mutagenesis was performed. We thank
31 Nick Brown, and the Kyoto and Bloomington Stock Centres for *Drosophila* strains, and Jessica
32 Gamage (née Allen) and Pablo Barrecheguren for their help in the mutagenesis screen. This work
33 was supported by grants from the Ministerio de Ciencia e Innovación (BFU2011-25828 and
34 “Ramón y Cajal” fellowship award) and a Marie Curie Career Integration Grant (PCIG09-GA-
35 2011-293479).

1
2
3
4
5
6
7
8
9
10
11
12
13
14
15
16
17
18
19
20
21
22
23
24
25
26
27
28
29
30
31
32
33
34
35
36

Author contributions

NG conceived the project. JdN designed and performed the mutagenesis screen. JJ and NG performed all other experiments, analysed the data and discussed the results. NG wrote the manuscript, with feedback from JdN. All authors corrected and approved the final manuscript.

Conflict of interest

The authors declare they have no conflict of interest.

Figure legends

Figure 1. Characterization of α -Catenin alleles. (A) Schematic representation of α -Catenin genomic region of the chromosome used for the mutagenesis. Note that only one transcript is represented for each of the three loci of the region. (B) Schematic representation of α -Catenin mutant proteins. (C) Sequence alignment of the C-terminal region of α -Catenin. (D) Homozygote mutant clones for the different α -Catenin alleles in wing imaginal discs. (i-i'') Low magnification of wing imaginal discs with the location of the clone indicated. (ii-ii'') Staining for α -Catenin. (iii-iii'') The clones are visualized by the lack of GFP, is indicated with a dotted line. (iv-iv'') DAPI signal to label nuclei. (v-v'') Merge. (E-F) Immunoblot of α -Catenin in α -Catenin stage 13 mutant embryos. (G) Quantification of α -Catenin signal from 4 independent experiments. Data show the mean +/- Standard Error and the following statistical significance from unpaired t-test comparison: *** $p \leq 0.001$; ** $p \leq 0.01$; * $p \leq 0.05$. (H-L) Cuticles of wild-type (H) and different categories of mutant (I-L) embryos. (M) Quantification of cuticle defects. (N) Statistical differences in the proportion of each phenotypic category between our mutant alleles and the null allele. Scale bars are 100 μm in Di-i'' and G-K; 10 μm in Dii-v'.

Figure 2. Live imaging of α -Catenin mutant embryos. (A) Still images of example DE-Cadherin::GFP (i-iv) and DE-Cadherin::GFP; α -Cat^{l3} (i'-iv') embryos at the indicated times (similar defects were observed for the other alleles). The dorsal ridge is indicated in yellow and a hole is indicated with a purple dotted line. The width of the AS is indicated with a red line (i). The red dotted line indicates the length of the AS (i') and was used as a reference to calculate the half-width of the AS when one leading edge was out of the plane of view. (B) Quantification of the width of the AS at its symmetry axis in 7 wild-type versus 5 α -Cat^l (i), 5 α -Cat^{l3} (ii), 4 α -Cat²⁰⁴⁹

1 (iii) and 5 α -Cat⁴²¹ (iv) mutant embryos. The curve corresponding to the wild-type is always shown
2 in black. Linear regression analysis was done to get the velocity of DC progression from 50 min.
3 onwards and compared each mutant allele with the wild-type using unpaired t-test comparison. p-
4 values are indicated in each graph. (C) Number of AS cells at time 0 of DC and (D) number of cell
5 delamination events in wild-type and α -Catenin mutant embryos. Each dot shows data per embryo.
6 The mean (thick line) and standard deviation (thin lines) are indicated; the mean per genotype was
7 compared to the -type using unpaired t-test comparison: ***p \leq 0.001; **p \leq 0.01; *p \leq 0.05. Scale bar
8 is 50 μ m in A.

9
10 Figure 3. Apical cell area oscillations in AS cells of α -Catenin mutant embryos. (A) Still images
11 from a time-lapse movie of example DE-Cadherin::GFP (i-iii) and α -Cat⁴²¹ (i'-iii') embryos at 90',
12 150' and 210' of DC. (Similar dynamics was observed for the other alleles). (B-E) Analysis of cell
13 area fluctuations in data pooled from 7 wild-type (i-i'''), 4 α -Cat¹³ (ii-ii'''), 4 α -Cat²⁰⁴⁹ (iii-iii''') and
14 5 α -Cat⁴²¹ (iv-iv''') embryos. (B) Average cycle length of AS cells as a function of their location
15 along the antero-posterior (AP) axis over time. Anterior is to the left in all similar panels. Cartoon
16 of cycle length (v). Statistical comparison of the cycle length of apical cell area oscillations
17 between the wild-type and the different α -Catenin alleles (vi-viii). (C) Average oscillation
18 amplitude as a function of AP location over time. Note the amplitude of oscillations is a
19 proportional measure expressed as the percentage of the apical cell area. Cartoon showing
20 amplitude (v'). Statistical comparison of the amplitude of apical cell area oscillations between the
21 wild-type and the different α -Catenin alleles (vi-viii). (D) Average contraction half-cycle duration
22 as a function of AP location over time. Cartoon of contraction half-cycle (v''). Statistical
23 comparison of the contraction half-cycle duration between the wild-type and the different α -
24 Catenin alleles (vi-viii). (E) Average expansion half-cycle duration as a function of their AP
25 location over time. Cartoon of expansion half-cycle (v'''). Statistical comparison of the expansion
26 half-cycle duration between the wild-type and the different α -Catenin alleles (vi-viii). In these and
27 in the following similar plots, the shaded area corresponds to regions of significant differences
28 applying a linear-mixed effect model (see Materials and Methods). Continuous and dotted white
29 lines in wild-type panels (B-E) indicates the transition different oscillatory modes. Scale bar is 50
30 μ m.

31
32 Figure 4. Dynamics of actin foci in AS cells in α -Catenin mutant embryos. (A) Still images of
33 example sGMCA (i-vi) and sGMCA; α -Cat¹³ (i'-vi') embryos, with actin foci indicated with
34 arrowheads in green. (B) Cartoon depicting the cycle length, duration, and time interval of a
35 schematic actomyosin focus. (C-D) Violin plots of the cycle length (B), duration (C) and time
36 interval between consecutive foci (D) from wild-type (188 foci from 6 embryos), α -Cat¹³ (158 foci

1 from 5 embryos), α -Cat²⁰⁴⁹ (112 foci from 4 embryos) and α -Cat⁴²¹ (86 foci from 5 embryos)
2 embryos. See also Table S1. Mean (diamond) and median (line) are indicated in the box-plot inside
3 each violin-plot. We performed a Mann-Whitney test to assess if the means for each mutant were
4 significantly different to control: ****p \leq 0.0001; ***p \leq 0.001; **p \leq 0.01; *p \leq 0.05. Scale bar is 10
5 μ m.

6
7 Figure 5. Dynamics of actin foci in AS cells in *shg* mutant embryos. (A) Still images of an example
8 sGMCA; *shg*^{g317} embryo (i-vi), with actin foci indicated with arrowheads in green. (B-D) Violin
9 plots of the cycle length (B), duration (C) and time interval between consecutive foci (D) from
10 *shg*^{g317} mutants (40 foci from 4 embryos). See also Table S1. (E-I) FRAP analysis of DE-
11 Cadherin::GFP (11 cells from 7 early and 13 cells from 7 late embryos) (E) and α -Catenin::YFP
12 (12 cells from 5 early and 18 cells from 8 late embryos) (G) in the AS of DC embryos during early
13 and late stages of DC. Note the reduction on the mobile fraction of both proteins as DC progresses.
14 In α -Cat²⁰⁴⁹ mutant embryos (12 cells from 8 early and 14 cells from 7 late embryos), there is no
15 decrease in the mobile fraction of DE-Cadherin::GFP (H). In α -Cat⁴²¹ mutant embryos (17 cells
16 from 6 early and 10 cells from 5 late embryos), there is a reduction in the mobile fraction of DE-
17 Cadherin::GFP (I). Comparisons between early and late mobile fractions show the following
18 statistical significance from unpaired t-test comparison: ***p \leq 0.001; **p \leq 0.01; *p \leq 0.05. Scale bar
19 is 10 μ m.

20
21 Figure 6. Interaction between α -Catenin and Vinculin and the actomyosin cytoskeleton. (A)
22 Quantification of the cuticle defects from embryos double homozygote for Vinculin and the
23 different α -Catenin alleles. (B) Quantification of the cuticle defects from α -Catenin mutant
24 embryos in which Sqh^{DD} is ectopically expressed in the AS. (C) Statistical differences in the
25 proportion of each phenotypic category between each mutant allele and the null allele. (D)
26 Localisation of Vinculin::GFP in AS cells from early and late DC stages (i-ii). (E) Localisation of
27 E-Cadherin::mTomato (i') and Vinculin::GFP (ii') in early DC embryos in which a constitutive
28 active form of MLCK has been ectopically expressed in the AS. (F) Localisation of Vinculin::GFP
29 in AS cells from early (i,i') and late ii,ii') DC stages in α -Cat²⁰⁴⁹ (i,ii) and α -Cat⁴²¹ (i',ii') embryos.
30 Scale bar is 25 μ m.

31 32 **Bibliography**

33
34 Benjamin, J.M., Kwiatkowski, A.V., Yang, C., Korobova, F., Pokutta, S., Svitkina, T., Weis, W.I.,
35 and Nelson, W.J. (2010). AlphaE-catenin regulates actin dynamics independently of cadherin-
36 mediated cell-cell adhesion. *The Journal of cell biology* 189, 339-352.

1 Blanchard, G.B., Kabla, A.J., Schultz, N.L., Butler, L.C., Sanson, B., Gorfinkiel, N., Mahadevan,
2 L., and Adams, R.J. (2009). Tissue tectonics: morphogenetic strain rates, cell shape change and
3 intercalation. *Nature methods* 6, 458-464.

4 Blanchard, G.B., Murugesu, S., Adams, R.J., Martinez-Arias, A., and Gorfinkiel, N. (2010).
5 Cytoskeletal dynamics and supracellular organisation of cell shape fluctuations during dorsal
6 closure. *Development (Cambridge, England)* 137, 2743-2752.

7 Borghi, N., Sorokina, M., Shcherbakova, O.G., Weis, W.I., Pruitt, B.L., Nelson, W.J., and Dunn,
8 A.R. (2012). E-cadherin is under constitutive actomyosin-generated tension that is increased at
9 cell-cell contacts upon externally applied stretch. *Proceedings of the National Academy of Sciences*
10 *of the United States of America* 109, 12568-12573.

11 Buckley, C.D., Tan, J., Anderson, K.L., Hanein, D., Volkmann, N., Weis, W.I., Nelson, W.J., and
12 Dunn, A.R. (2014). Cell adhesion. The minimal cadherin-catenin complex binds to actin filaments
13 under force. *Science* 346, 1254211.

14 Butler, L.C., Blanchard, G.B., Kabla, A.J., Lawrence, N.J., Welchman, D.P., Mahadevan, L.,
15 Adams, R.J., and Sanson, B. (2009). Cell shape changes indicate a role for extrinsic tensile forces
16 in *Drosophila* germ-band extension. *Nature cell biology* 11, 859-864.

17 Cavey, M., Rauzi, M., Lenne, P.F., and Lecuit, T. (2008). A two-tiered mechanism for stabilization
18 and immobilization of E-cadherin. *Nature* 453, 751-756.

19 Chen, C.S., Hong, S., Indra, I., Sergeeva, A.P., Troyanovsky, R.B., Shapiro, L., Honig, B., and
20 Troyanovsky, S.M. (2015). alpha-Catenin-mediated cadherin clustering couples cadherin and actin
21 dynamics. *The Journal of cell biology* 210, 647-661.

22 Cheng, X., Li, F., Han, S., Zhang, Y., Jiao, C., Wei, J., Ye, K., Wang, Y., and Zhang, H. (2015).
23 Emission behaviors of unsymmetrical 1,3-diaryl-beta-diketones: a model perfectly disclosing the
24 effect of molecular conformation on luminescence of organic solids. *Sci Rep* 5, 9140.

25 David, D.J., Tishkina, A., and Harris, T.J. (2010). The PAR complex regulates pulsed actomyosin
26 contractions during amnioserosa apical constriction in *Drosophila*. *Development (Cambridge,*
27 *England)* 137, 1645-1655.

28 David, D.J., Wang, Q., Feng, J.J., and Harris, T.J. (2013). Bazooka inhibits aPKC to limit
29 antagonism of actomyosin networks during amnioserosa apical constriction. *Development*
30 *(Cambridge, England)* 140, 4719-4729.

31 Desai, R., Sarpal, R., Ishiyama, N., Pellikka, M., Ikura, M., and Tepass, U. (2013). Monomeric
32 alpha-catenin links cadherin to the actin cytoskeleton. *Nature cell biology* 15, 261-273.

33 Drees, F., Pokutta, S., Yamada, S., Nelson, W.J., and Weis, W.I. (2005). Alpha-catenin is a
34 molecular switch that binds E-cadherin-beta-catenin and regulates actin-filament assembly. *Cell*
35 *123*, 903-915.

36 Ellis, S.J., Goult, B.T., Fairchild, M.J., Harris, N.J., Long, J., Lobo, P., Czerniecki, S., Van
37 Petegem, F., Schock, F., Peifer, M., *et al.* (2013). Talin autoinhibition is required for
38 morphogenesis. *Curr Biol* 23, 1825-1833.

39 Fischer, S.C., Blanchard, G.B., Duque, J., Adams, R.J., Arias, A.M., Guest, S.D., and Gorfinkiel,
40 N. (2014). Contractile and mechanical properties of epithelia with perturbed actomyosin dynamics.
41 *PLoS One* 9, e95695.

42 Frischmeyer, P.A., and Dietz, H.C. (1999). Nonsense-mediated mRNA decay in health and disease.
43 *Hum Mol Genet* 8, 1893-1900.

44 Gorfinkiel, N. (2016). From actomyosin oscillations to tissue-level deformations. *Dev Dyn* 245,
45 268-275.

46 Gorfinkiel, N., Blanchard, G.B., Adams, R.J., and Martinez Arias, A. (2009). Mechanical control
47 of global cell behaviour during dorsal closure in *Drosophila*. *Development (Cambridge, England)*
48 *136*, 1889-1898.

49 Gorfinkiel, N., and Martínez Arias, A. (2007). Requirements for Adherens Junctions components
50 in the interaction between epithelial tissues during Dorsal Closure in *Drosophila*. *Journal of Cell*
51 *Sci* 120, 3289-3298.

52 Gorfinkiel, N., Schamberg, S., and Blanchard, G.B. (2011). Integrative approaches to
53 morphogenesis: lessons from dorsal closure. *Genesis* 49, 522-533.

54 Hara, Y., Shagirov, M., and Toyama, Y. (2016). Cell Boundary Elongation by Non-autonomous
55 Contractility in Cell Oscillation. *Curr Biol* 26, 2388-2396.

1 Hazan, R.B., Kang, L., Roe, S., Borgen, P.I., and Rimm, D.L. (1997). Vinculin is associated with
2 the E-cadherin adhesion complex. *The Journal of biological chemistry* 272, 32448-32453.

3 Heisenberg, C.P., and Bellaïche, Y. (2013). Forces in tissue morphogenesis and patterning. *Cell*
4 153, 948-962.

5 Hutson, M.S., Veldhuis, J., Ma, X., Lynch, H.E., Cranston, P.G., and Brodland, G.W. (2009).
6 Combining laser microsurgery and finite element modeling to assess cell-level epithelial
7 mechanics. *Biophys J* 97, 3075-3085.

8 Huvneers, S., and de Rooij, J. (2013). Mechanosensitive systems at the cadherin-F-actin interface.
9 *Journal of cell science* 126, 403-413.

10 Imamura, Y., Itoh, M., Maeno, Y., Tsukita, S., and Nagafuchi, A. (1999). Functional domains of
11 alpha-catenin required for the strong state of cadherin-based cell adhesion. *The Journal of cell*
12 *biology* 144, 1311-1322.

13 Jacinto, A., Woolner, S., and Martin, P. (2002). Dynamic analysis of dorsal closure in *Drosophila*:
14 from genetics to cell biology. *Developmental cell* 3, 9-19.

15 Kiehart, D.P., Galbraith, C.G., Edwards, K.A., Rickoll, W.L., and Montague, R.A. (2000). Multiple
16 forces contribute to cell sheet morphogenesis for dorsal closure in *Drosophila*. *The Journal of cell*
17 *biology* 149, 471-490.

18 Kim, T.J., Zheng, S., Sun, J., Muhamed, I., Wu, J., Lei, L., Kong, X., Leckband, D.E., and Wang,
19 Y. (2015). Dynamic visualization of alpha-catenin reveals rapid, reversible conformation switching
20 between tension states. *Curr Biol* 25, 218-224.

21 Klapholz, B., Herbert, S.L., Wellmann, J., Johnson, R., Parsons, M., and Brown, N.H. (2015).
22 Alternative mechanisms for talin to mediate integrin function. *Curr Biol* 25, 847-857.

23 le Duc, Q., Shi, Q., Blonk, I., Sonnenberg, A., Wang, N., Leckband, D., and de Rooij, J. (2010).
24 Vinculin potentiates E-cadherin mechanosensing and is recruited to actin-anchored sites within
25 adherens junctions in a myosin II-dependent manner. *The Journal of cell biology* 189, 1107-1115.

26 Lecuit, T., and Yap, A.S. (2015). E-cadherin junctions as active mechanical integrators in tissue
27 dynamics. *Nature cell biology* 17, 533-539.

28 Maiden, S.L., and Hardin, J. (2011). The secret life of alpha-catenin: moonlighting in
29 morphogenesis. *The Journal of cell biology* 195, 543-552.

30 Maiden, S.L., Harrison, N., Keegan, J., Cain, B., Lynch, A.M., Pettitt, J., and Hardin, J. (2013).
31 Specific conserved C-terminal amino acids of *Caenorhabditis elegans* HMP-1/alpha-catenin
32 modulate F-actin binding independently of vinculin. *The Journal of biological chemistry* 288,
33 5694-5706.

34 Martin, A.C., Kaschube, M., and Wieschaus, E.F. (2009). Pulsed contractions of an actin-myosin
35 network drive apical constriction. *Nature* 457, 495-499.

36 Meghana, C., Ramdas, N., Hameed, F.M., Rao, M., Shivashankar, G.V., and Narasimha, M.
37 (2011). Integrin adhesion drives the emergent polarization of active cytoskeletal stresses to pattern
38 cell delamination. *Proceedings of the National Academy of Sciences of the United States of*
39 *America* 108, 9107-9112.

40 Mulyil, S., Krishnakumar, P., and Narasimha, M. (2011). Spatial, temporal and molecular
41 hierarchies in the link between death, delamination and dorsal closure. *Development (Cambridge,*
42 *England)* 138, 3043-3054.

43 Munjal, A., Philippe, J.M., Munro, E., and Lecuit, T. (2015). A self-organized biomechanical
44 network drives shape changes during tissue morphogenesis. *Nature* 524, 351-355.

45 Narasimha, M., and Brown, N.H. (2004). Novel functions for integrins in epithelial morphogenesis.
46 *Curr Biol* 14, 381-385.

47 Pacquelet, A., and Rorth, P. (2005). Regulatory mechanisms required for DE-cadherin function in
48 cell migration and other types of adhesion. *The Journal of cell biology* 170, 803-812.

49 Reed, B.H., Wilk, R., Schock, F., and Lipshitz, H.D. (2004). Integrin-dependent apposition of
50 *Drosophila* extraembryonic membranes promotes morphogenesis and prevents anoikis. *Curr Biol*
51 14, 372-380.

52 Roh-Johnson, M., Shemer, G., Higgins, C.D., McClellan, J.H., Werts, A.D., Tulu, U.S., Gao, L.,
53 Betzig, E., Kiehart, D.P., and Goldstein, B. (2012). Triggering a cell shape change by exploiting
54 preexisting actomyosin contractions. *Science* 335, 1232-1235.

1 Ryder, E., Blows, F., Ashburner, M., Bautista-Llacer, R., Coulson, D., Drummond, J., Webster, J.,
2 Gubb, D., Gunton, N., Johnson, G., *et al.* (2004). The DrosDel collection: a set of P-element
3 insertions for generating custom chromosomal aberrations in *Drosophila melanogaster*. *Genetics*
4 *167*, 797-813.

5 Sarpal, R., Pellikka, M., Patel, R.R., Hui, F.Y., Godt, D., and Tepass, U. (2012). Mutational
6 analysis supports a core role for *Drosophila* alpha-catenin in adherens junction function. *Journal of*
7 *cell science* *125*, 233-245.

8 Schuldiner, O., Berdnik, D., Levy, J.M., Wu, J.S., Luginbuhl, D., Gontang, A.C., and Luo, L.
9 (2008). piggyBac-based mosaic screen identifies a postmitotic function for cohesin in regulating
10 developmental axon pruning. *Developmental cell* *14*, 227-238.

11 Solon, J., Kaya-Copur, A., Colombelli, J., and Brunner, D. (2009). Pulsed forces timed by a
12 ratchet-like mechanism drive directed tissue movement during dorsal closure. *Cell* *137*, 1331-1342.

13 Tepass, U., Gruszynski-DeFeo, E., Haag, T.A., Omatyar, L., Torok, T., and Hartenstein, V. (1996).
14 shotgun encodes *Drosophila* E-cadherin and is preferentially required during cell rearrangement in
15 the neurectoderm and other morphogenetically active epithelia. *Genes & development* *10*, 672-685.

16 Thibault, S.T., Singer, M.A., Miyazaki, W.Y., Milash, B., Dompe, N.A., Singh, C.M., Buchholz,
17 R., Demsky, M., Fawcett, R., Francis-Lang, H.L., *et al.* (2004). A complementary transposon tool
18 kit for *Drosophila melanogaster* using P and piggyBac. *Nat Genet* *36*, 283-287.

19 Tornavaca, O., Chia, M., Dufton, N., Almagro, L.O., Conway, D.E., Randi, A.M., Schwartz, M.A.,
20 Matter, K., and Balda, M.S. (2015). ZO-1 controls endothelial adherens junctions, cell-cell tension,
21 angiogenesis, and barrier formation. *The Journal of cell biology* *208*, 821-838.

22 Toyama, Y., Peralta, X.G., Wells, A.R., Kiehart, D.P., and Edwards, G.S. (2008). Apoptotic force
23 and tissue dynamics during *Drosophila* embryogenesis. *Science* *321*, 1683-1686.

24 VanHook, A., and Letsou, A. (2008). Head involution in *Drosophila*: genetic and morphogenetic
25 connections to dorsal closure. *Dev Dyn* *237*, 28-38.

26 Vasquez, C.G., Tworoger, M., and Martin, A.C. (2014). Dynamic myosin phosphorylation
27 regulates contractile pulses and tissue integrity during epithelial morphogenesis. *The Journal of cell*
28 *biology* *206*, 435-450.

29 Wang, Q., Feng, J.J., and Pismen, L.M. (2012). A cell-level biomechanical model of *Drosophila*
30 dorsal closure. *Biophysical journal* *103*, 2265-2274.

31 Wells, A.R., Zou, R.S., Tulu, U.S., Sokolow, A.C., Crawford, J.M., Edwards, G.S., and Kiehart,
32 D.P. (2014). Complete canthi removal reveals that forces from the amnioserosa alone are sufficient
33 to drive dorsal closure in *Drosophila*. *Molecular biology of the cell* *25*, 3552-3568.

34 Yamada, S., Pokutta, S., Drees, F., Weis, W.I., and Nelson, W.J. (2005). Deconstructing the
35 cadherin-catenin-actin complex. *Cell* *123*, 889-901.

36 Yao, M., Qiu, W., Liu, R., Efremov, A.K., Cong, P., Seddiki, R., Payre, M., Lim, C.T., Ladoux, B.,
37 Mege, R.M., *et al.* (2014). Force-dependent conformational switch of alpha-catenin controls
38 vinculin binding. *Nat Commun* *5*, 4525.

39 Yap, A.S., Gomez, G.A., and Parton, R.G. (2015). Adherens Junctions Revisualized: Organizing
40 Cadherins as Nanoassemblies. *Developmental cell* *35*, 12-20.

41 Yonemura, S., Wada, Y., Watanabe, T., Nagafuchi, A., and Shibata, M. (2010). alpha-Catenin as a
42 tension transducer that induces adherens junction development. *Nature cell biology* *12*, 533-542.

43

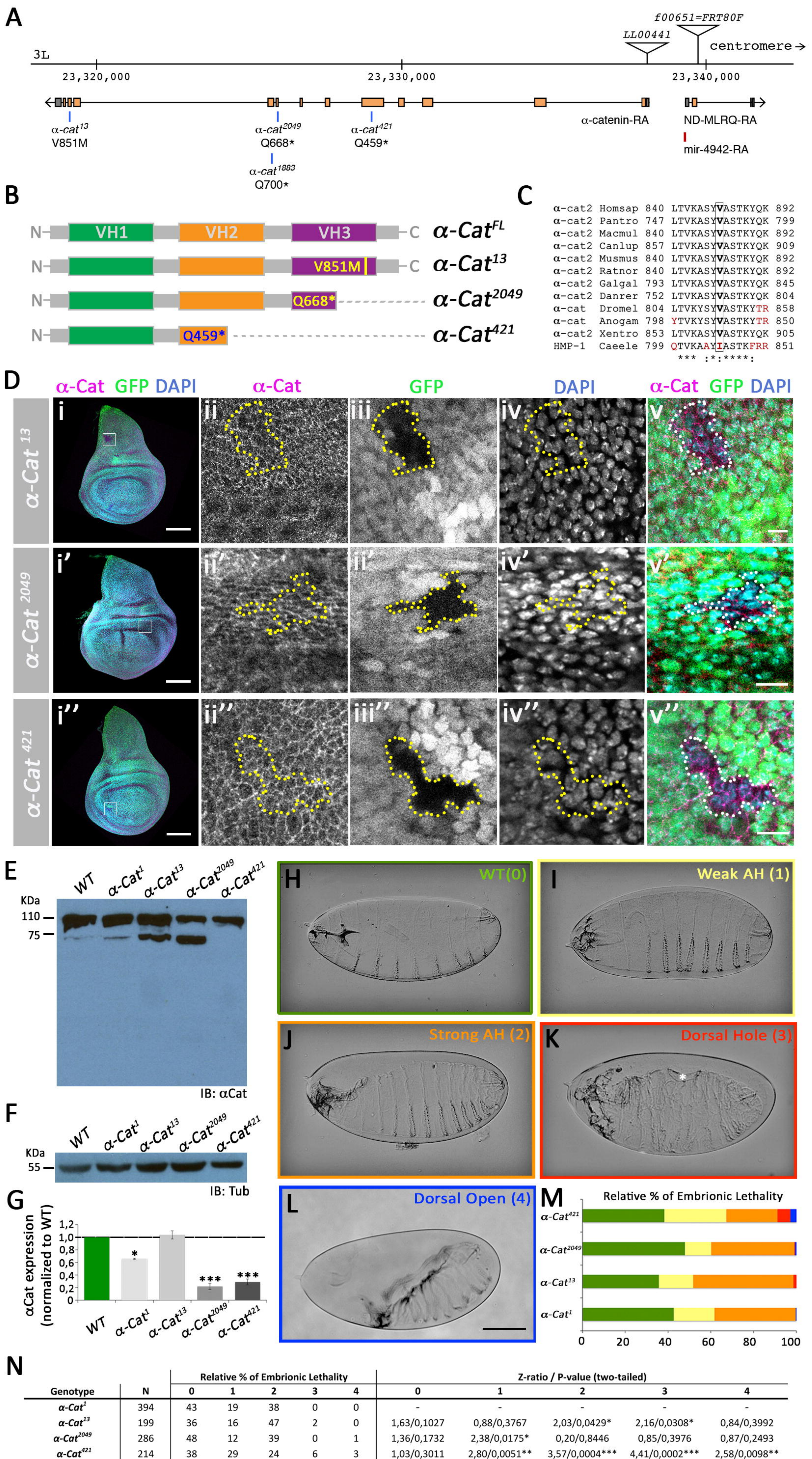


Fig. 1

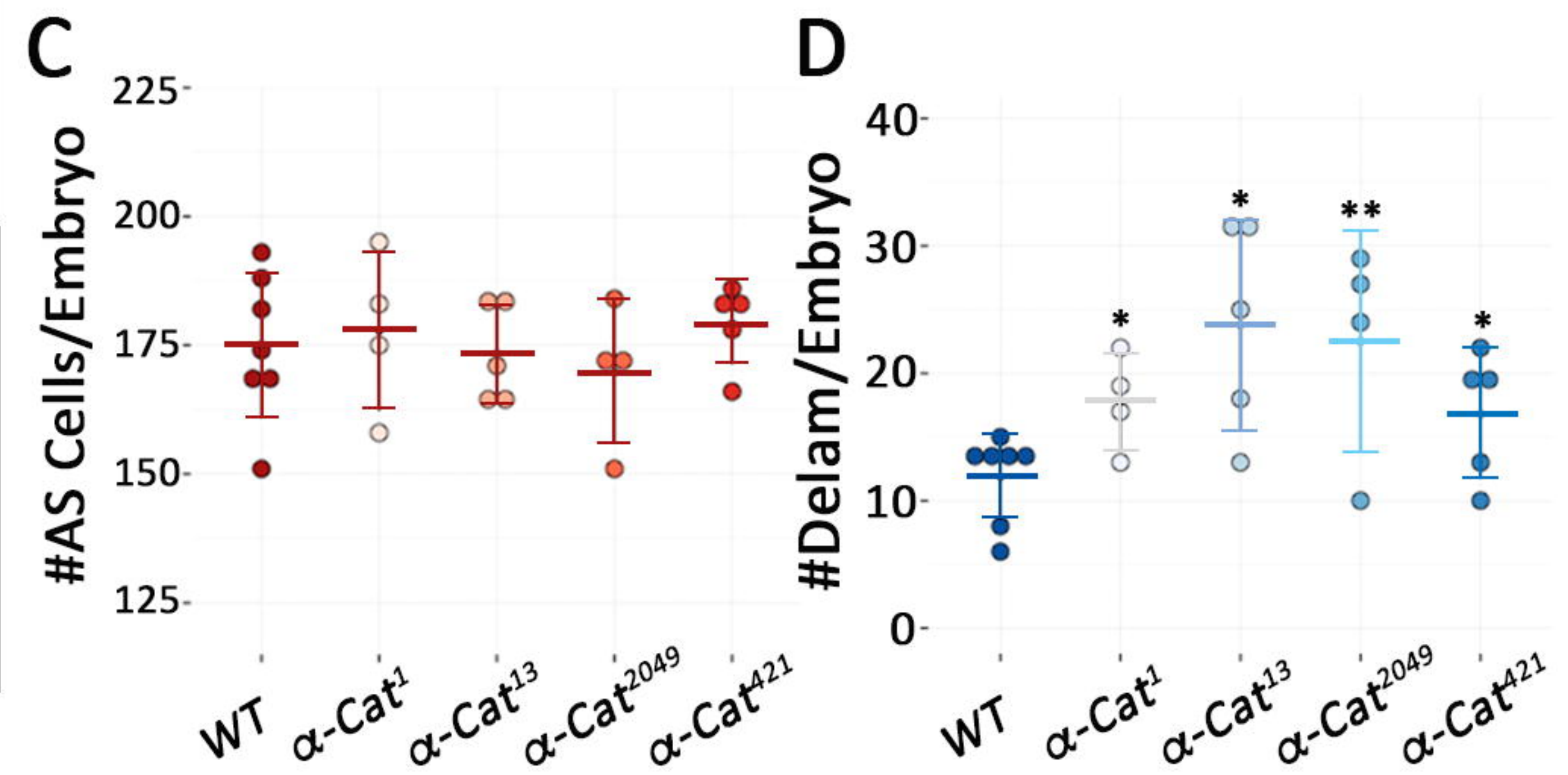
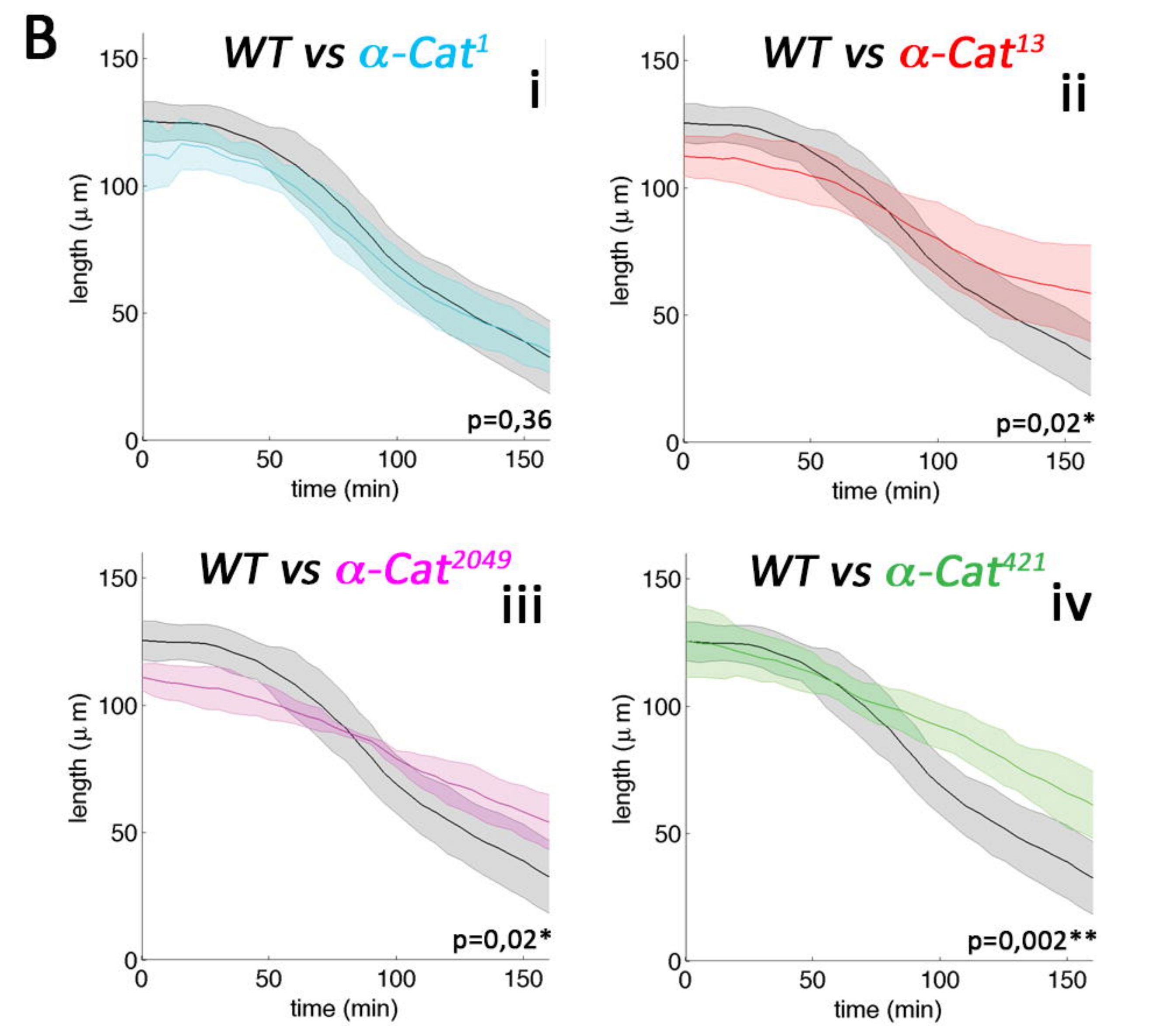
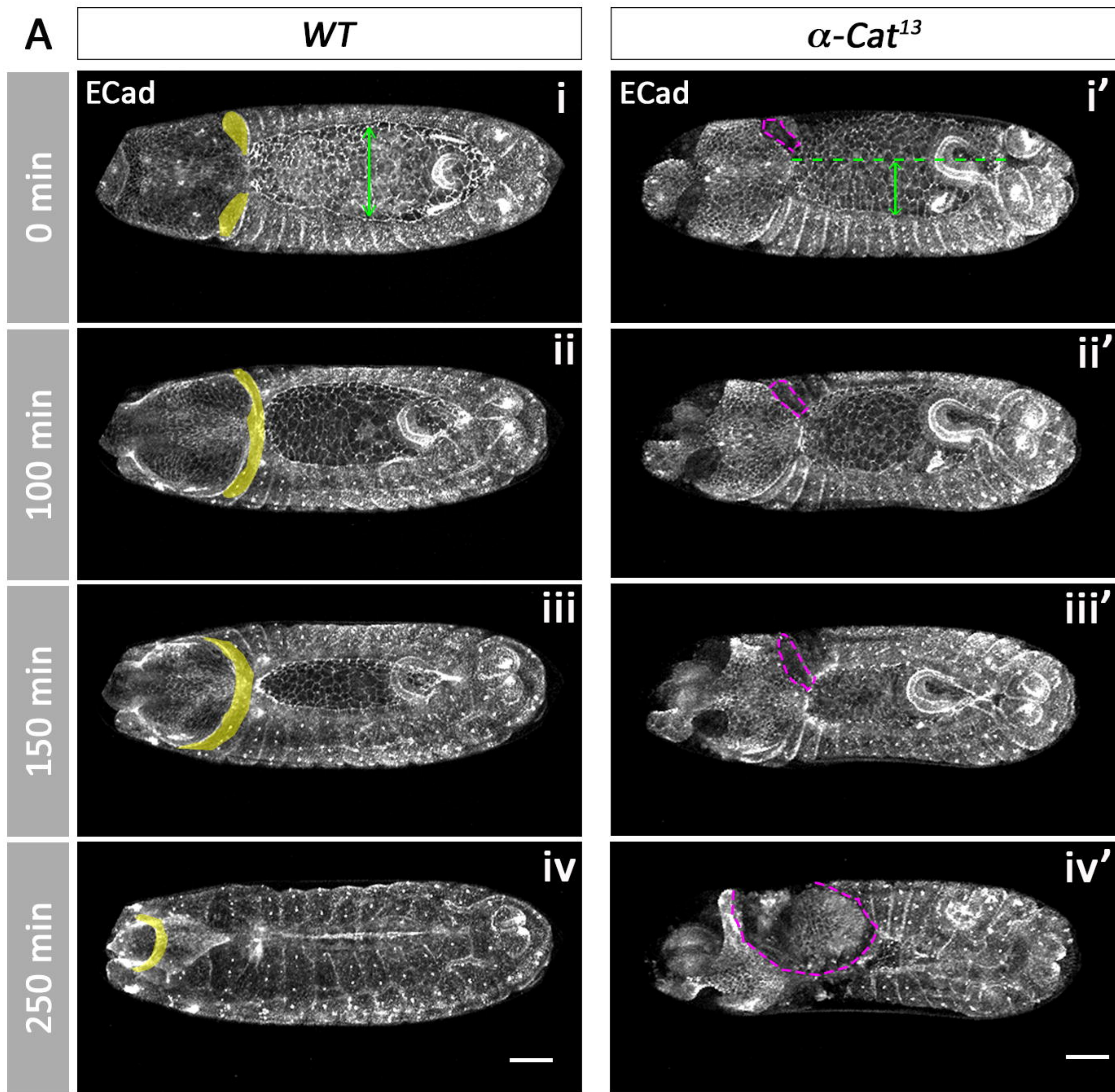


Fig. 2

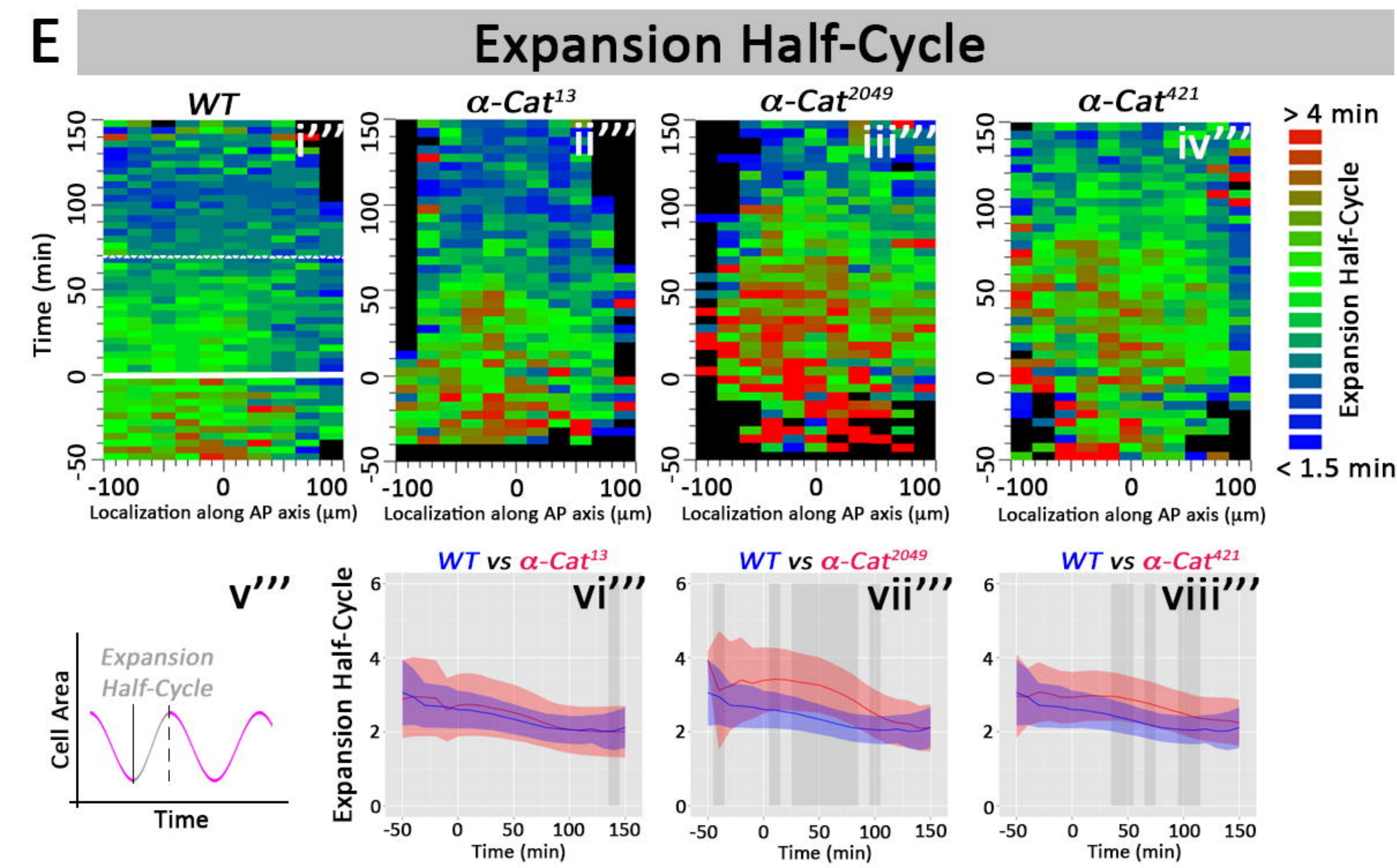
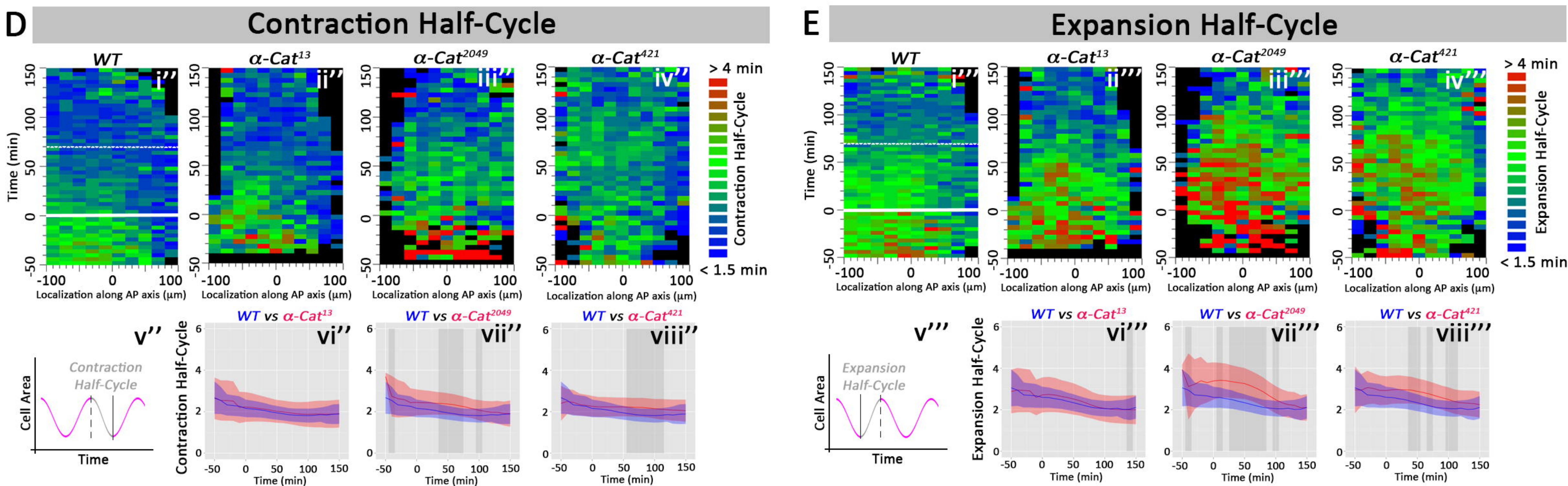
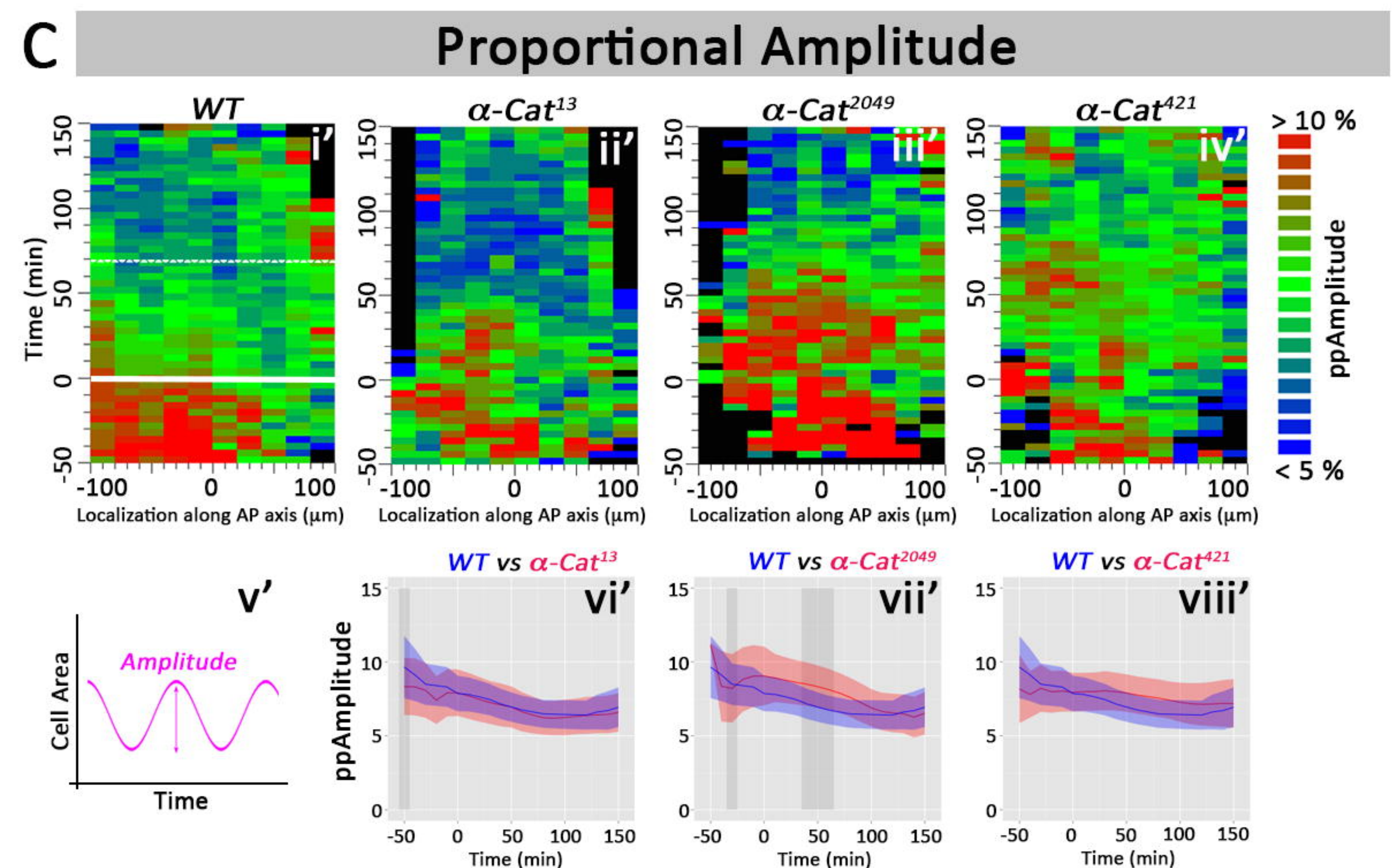
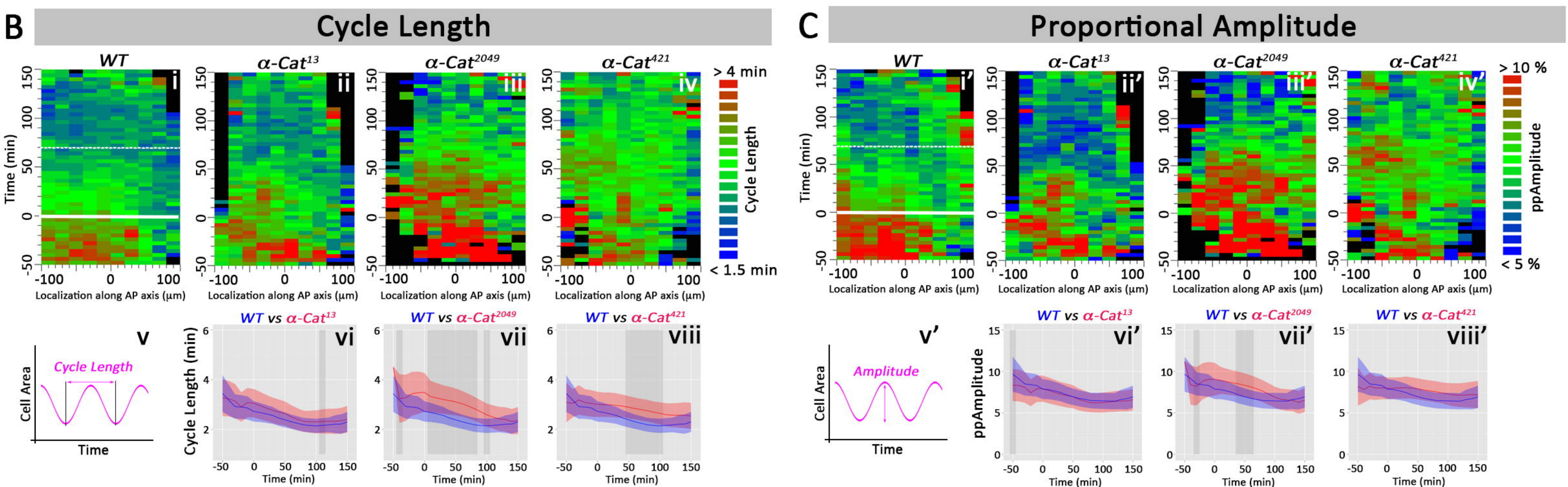
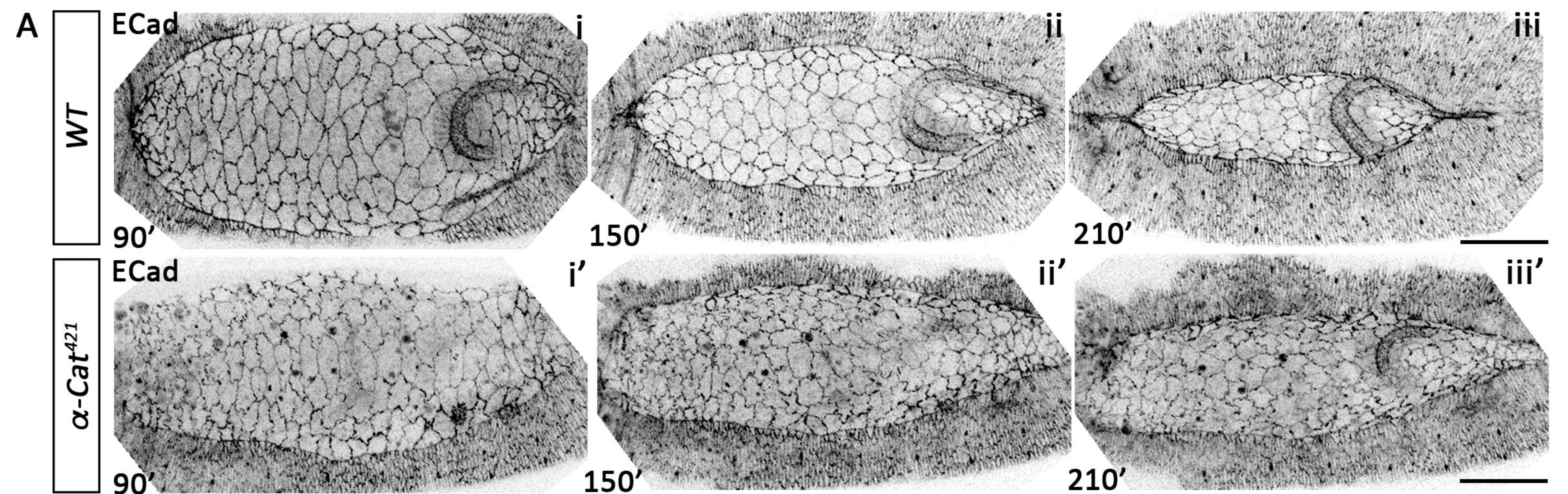


Fig. 3

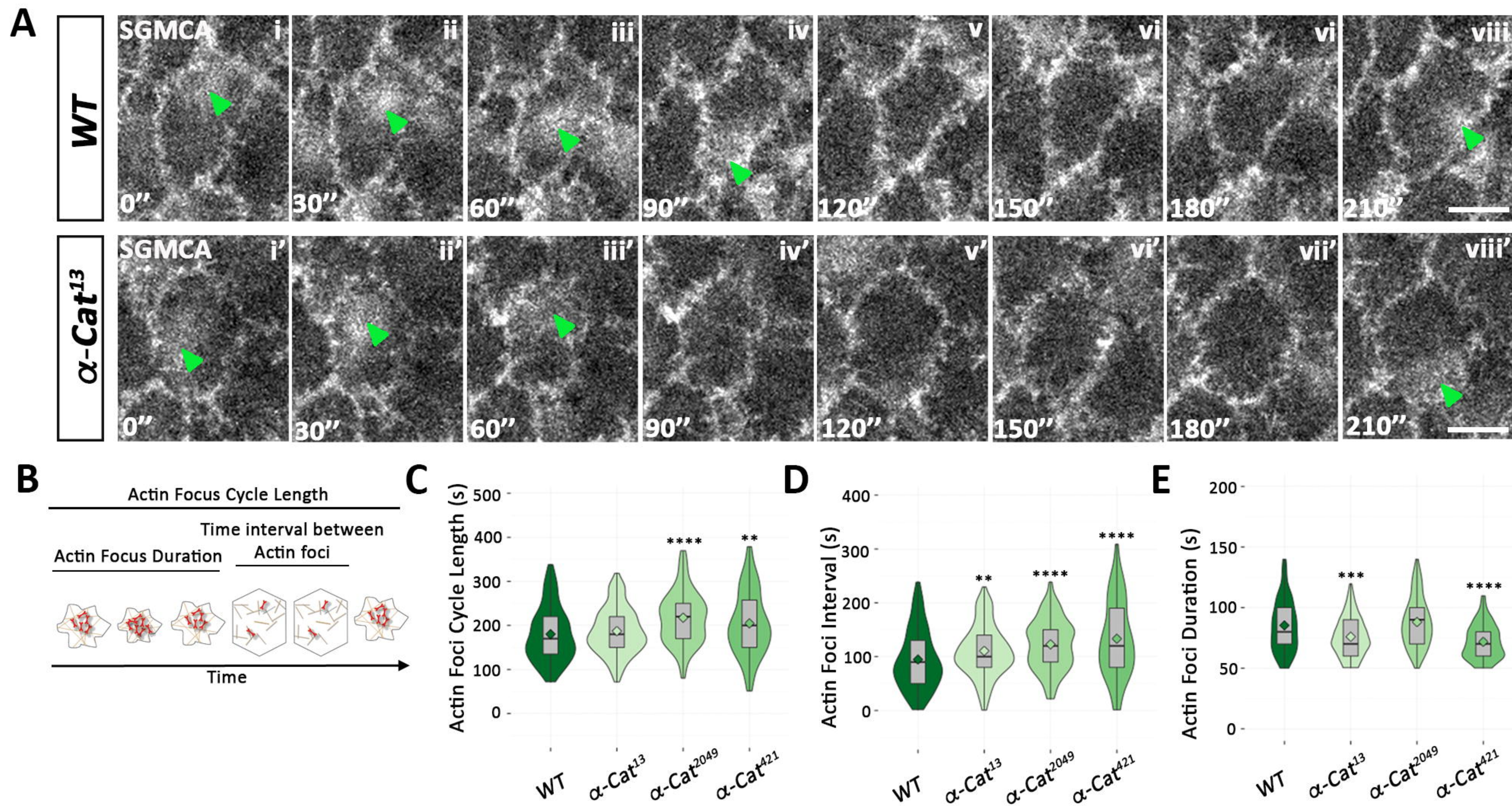


Fig. 4

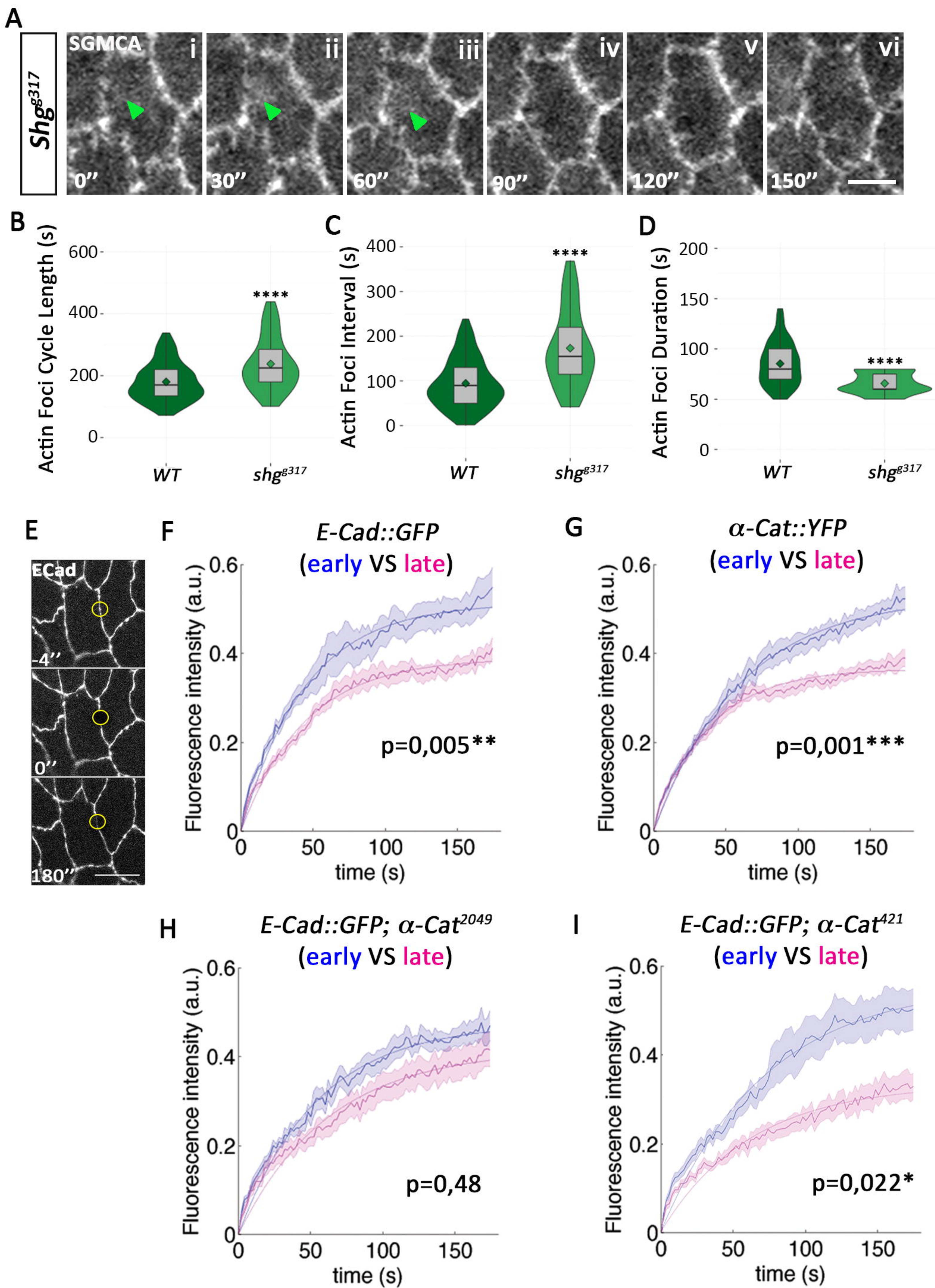


Fig. 5

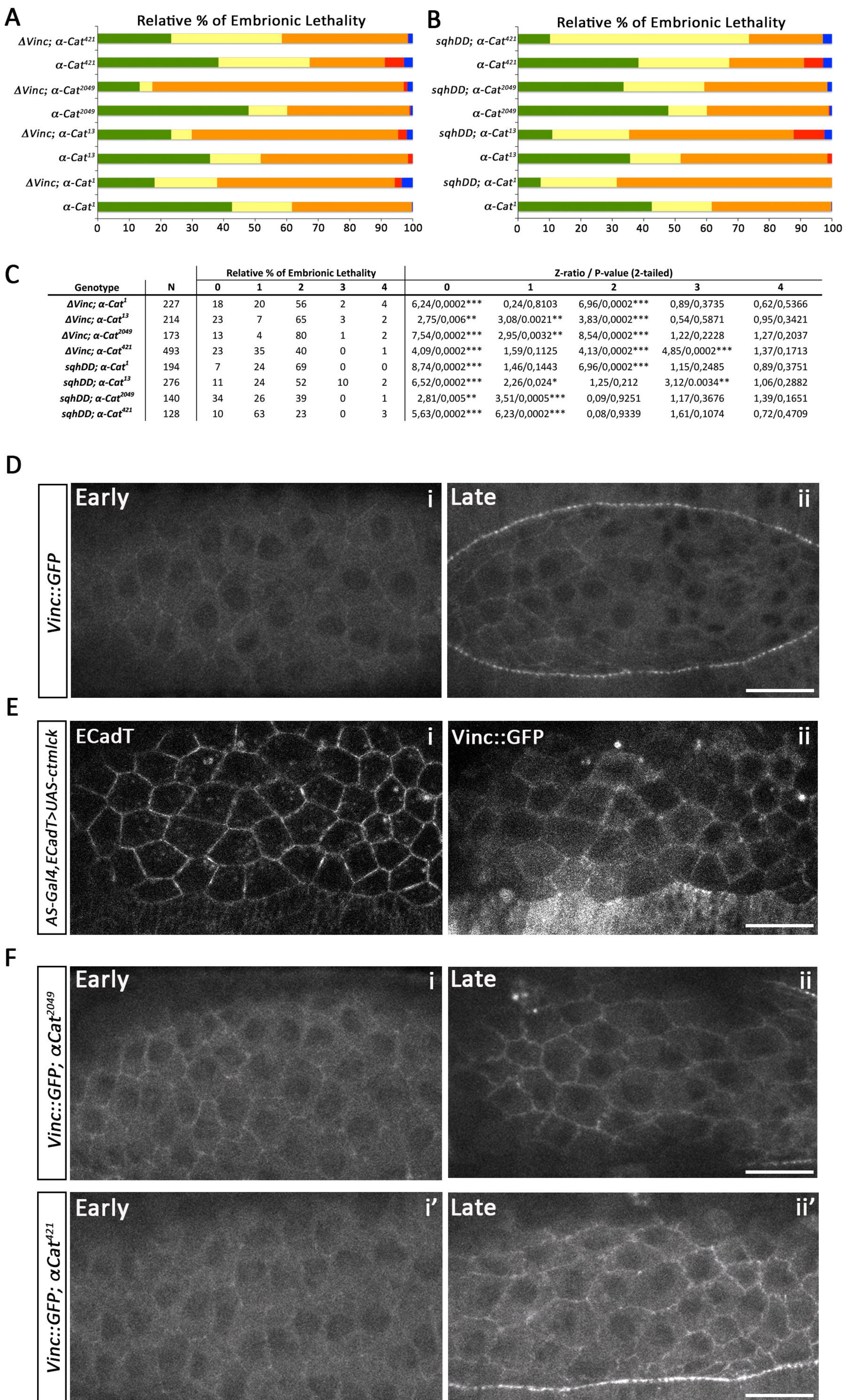


Fig. 6

Supplementary Material

α -Catenin stabilises Cadherin-Catenin complexes and modulates actomyosin dynamics to allow pulsatile apical contraction during dorsal closure

Jaime Jurado¹, Joaquín de Navascués² and Nicole Gorfinkiel¹

¹Centro de Biología Molecular “Severo Ochoa”, CSIC-UAM, Cantoblanco, Madrid, Spain.

²European Cancer Stem Cell Research Institute, School of Biosciences, Cardiff University, Cardiff CF24 4HQ, UK.

*Author for correspondence (email: ngorfinkiel@cbm.csic.es)

Supplementary figure and table legends

Figure S1. Staging of wild type and *a-Catenin* mutant embryos. Individual embryos were staged according to the evolution of four stereotypical parameters: cell area (i-iv), cell axial elongation - positive is oriented in the mediolateral direction- (i'-iv'), cell length in the mediolateral direction (i''-iv''), cumulative tissue strain rate (i'''-iv'''). The average shape behaviour \pm Standard Error for each genotype is shown in v-v''''.

Figure S2. (A) Quantification of the width of the amnioserosa at its symmetry axis in wild type and *a-Cat*¹ (i,ii) and *a-Cat*⁴²¹ (iii-iv) mutant embryos without (i,iii) and with (ii,iv) anterior holes (AH). The curve corresponding to the wild type is always shown in black. Linear regression analysis was done to get the velocity of DC progression from 50 min. onwards and compared each group with the wild type using unpaired t-test comparison. p-values are indicated in each graph. In *a-Cat*¹ mutant embryos, the presence of an anterior hole does not slow down DC progression, while the absence of an anterior hole in *a-Cat*⁴²¹ mutant embryos still slows down DC progression. (B) Disorganization of the actin cable in *a-Catenin* mutant embryos. Immunostaining of dorsal closure heterozygote *a-Cat*¹ (i-iii), homozygote *a-Cat*¹ (i'-iii'), *a-Cat*¹³ (i''-iii''), *a-Cat*²⁰⁴⁹ (i'''-iii''') and *a-Cat*⁴²¹ (i''''-iii''''') embryos stained for E-Cadherin (ii-ii''''') and F-actin (iii-iii'''''). Notice the defective localisation of DE-Cadherin at the leading edge in the mutants. Quantification of mean F-actin fluorescence from a region of (box in iii-iii''''') across the dorso-ventral axis (iv-iv'''''). Notice the decrease in the intensity peak in mutant embryos (magenta arrows). Scale bars are 50 μ m (i-i''''') and 10 μ m (iii-iii''''').

Figure S3. (A) Statistical analysis of cell shape oscillations: Log ratio of expansion to contraction half-cycle durations over time from wild-type (blue) and *a-Cat*¹³ (i, red), *a-Cat*²⁰⁴⁹ (ii, red) and *a-Cat*⁴²¹ (iii, red) mutant embryos. (B) Statistical analysis of cell strain rate: Proportional rate of contraction of AS cells over time from wild-type (blue) and *a-Cat*¹³ (i, red), *a-Cat*²⁰⁴⁹ (ii, red) and

*a-Cat*⁴²¹ (iii, red) mutant embryos. (C) Statistical analysis of cell shape: Log ratio of cell perimeter to apical cell radius of AS cells over time from wild type (blue) and *a-Cat*¹³ (i, red), *a-Cat*²⁰⁴⁹ (ii, red) and *a-Cat*⁴²¹ (iii, red) mutant embryos.

Figure S4. Tension-dependent localisation of a Vinculin reporter. Still images from c381Gal4, ECad::mT>UAS-Vinculin::YFP (A), c381Gal4, ECad::mT>UAS-Vinculin::YFP>UAS-MbsN300 (B) and c381Gal4, ECad::mT>UAS-Vinculin::YFP>UAS-ctMLCK (C), during early (i-iv") and late (v-viii") DC embryos. Scale bar is 25 μ m.

Table S1. Actin foci dynamics (mean value \pm Standard Deviation / p-value) in AS cells from wild type, *a-Catenin* and *shg*^{g317} mutant embryos.

Table S2. List of stocks used in this work.

Supplementary movie legends (Due to space constraints we don't show all the movies used in this manuscript.)

Movie 1. Time-lapse movie of a DE-Cadherin::GFP embryo during dorsal closure. Time interval: 180 seconds. Scale bar is 50 μ m.

Movie 2. Time-lapse movie of a DE-Cadherin::GFP; *a-Cat*¹³ embryo. Time interval: 180 seconds. Scale bar is 50 μ m.

Movie 3. Time-lapse movie of example DE-Cadherin::GFP; *a-Cat*¹³ (upper movie), DE-Cadherin::GFP; *a-Cat*²⁰⁴⁹ (middle movie) and DE-Cadherin::GFP; *a-Cat*⁴²¹ (lower movie) embryos. Time interval: 30 seconds. Scale bar is 50 μ m.

Movie 4. Time-lapse movie a wild type embryo during the slow phase carrying sGMCA reporter to visualize actin foci. Time interval: 10 seconds. Scale bar is 10 μ m.

Movie 5. Time-lapse movie a sGMCA; *a-Cat*¹³ embryo during the slow phase. Time interval: 10 seconds. Scale bar is 10 μ m.

Movie 6. Time-lapse movie of a sGMCA; *shg*^{g317} embryo during the slow phase. Time interval: 10 seconds. Scale bar is 10 μ m.

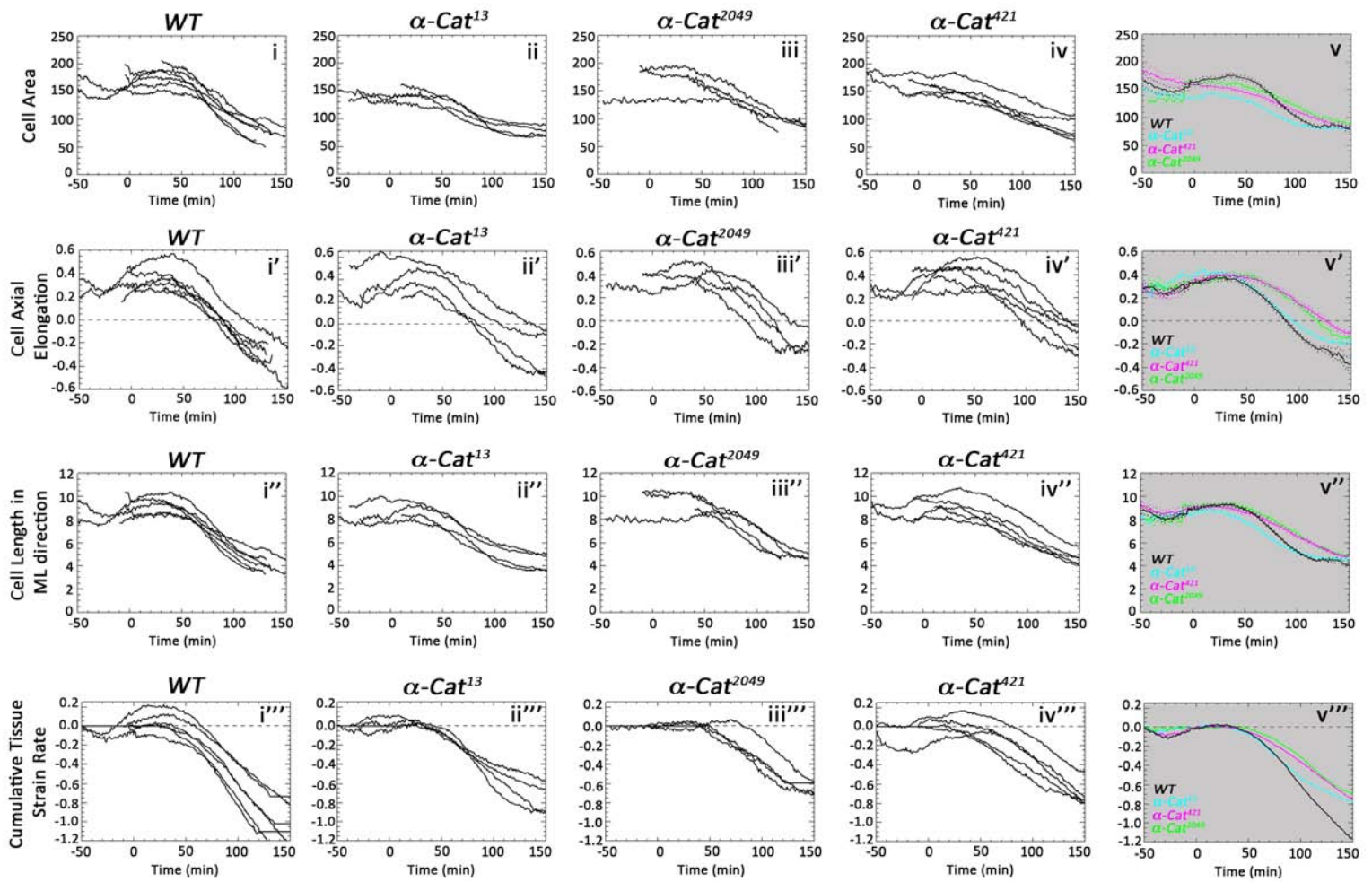


Fig. S1

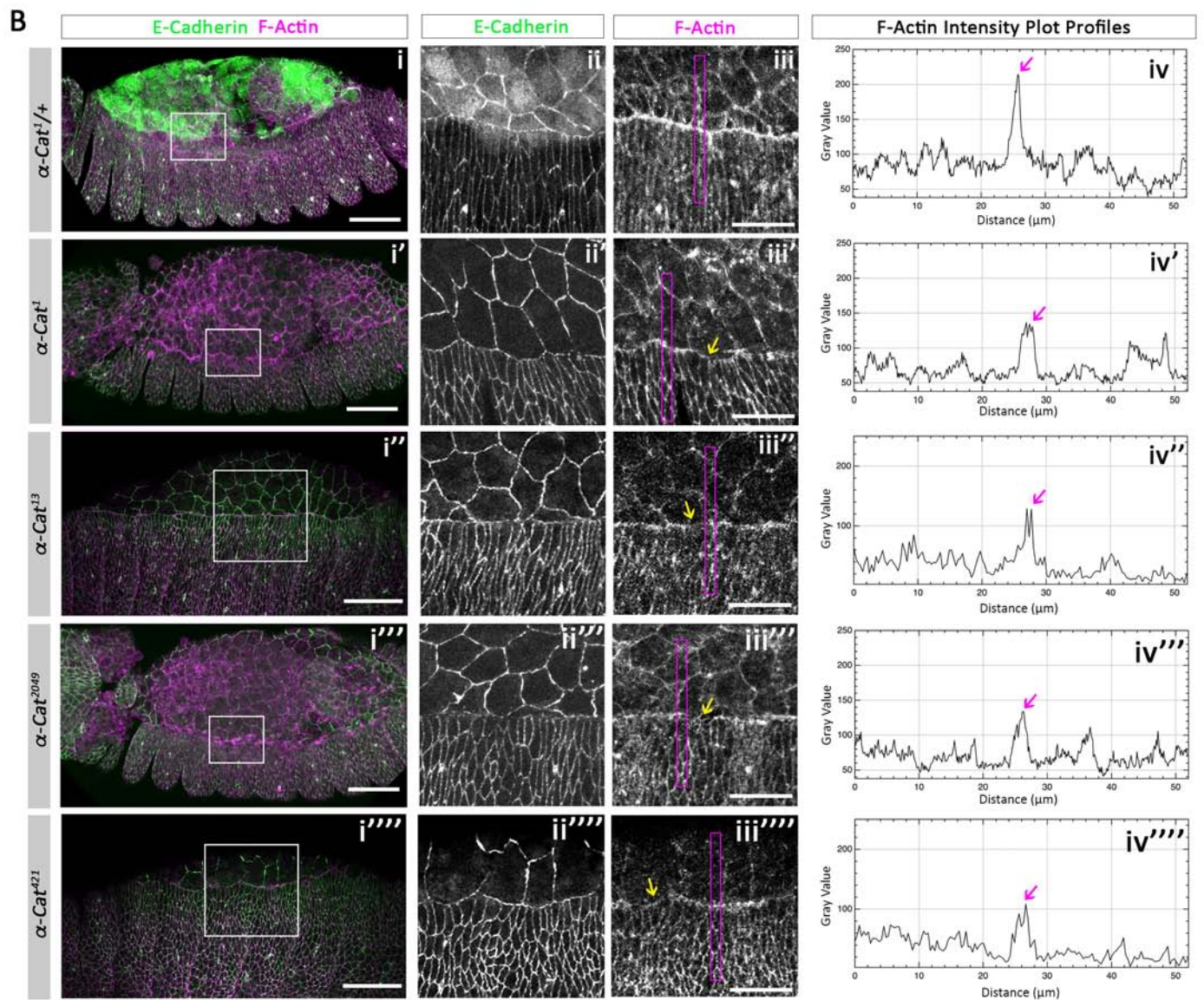
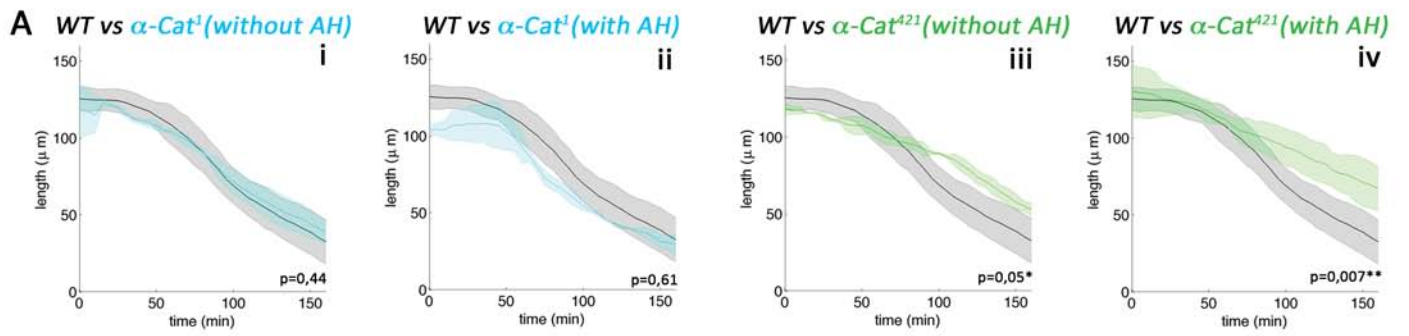


Fig. S2

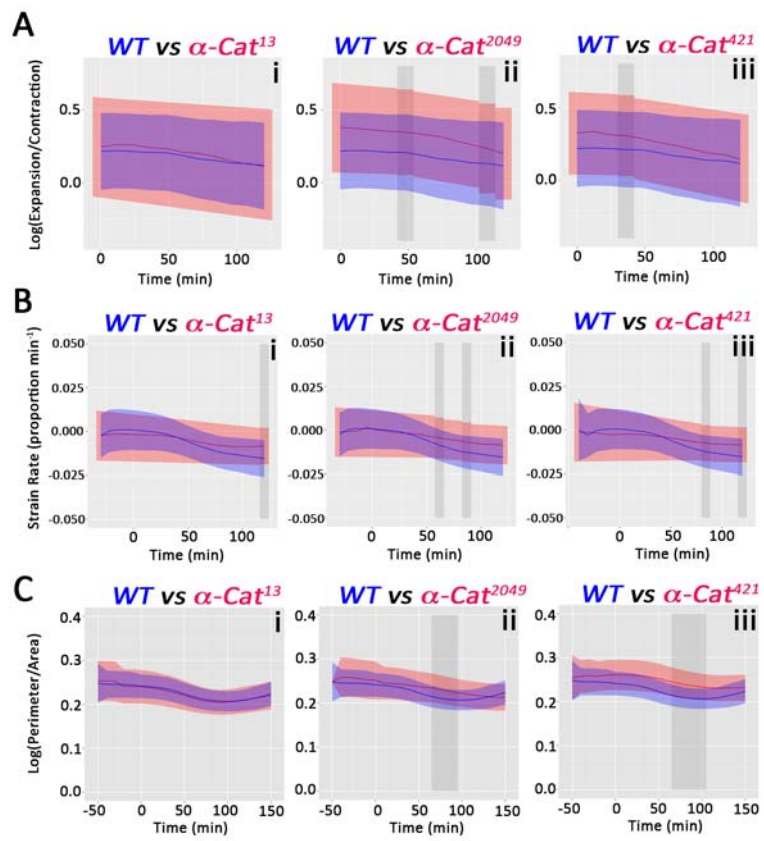


Fig. S3

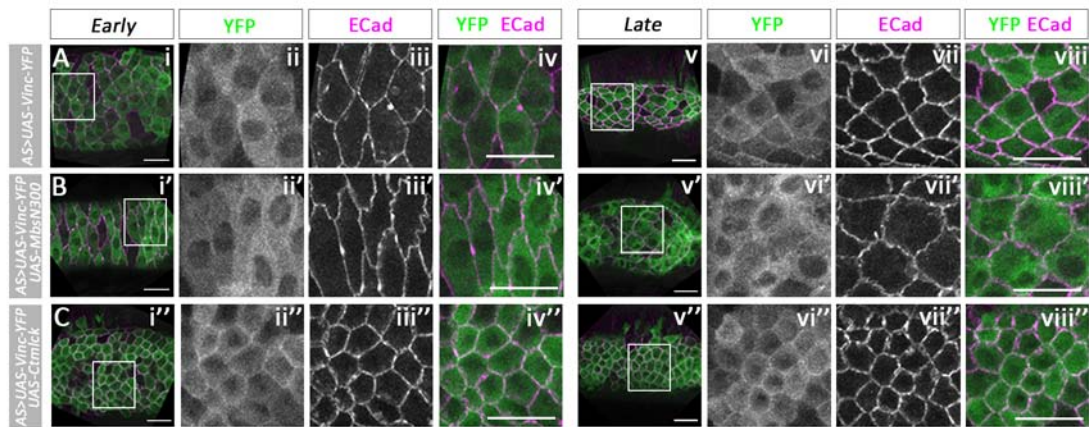


Fig. S4

Table S1.

Genotype	#Embryos	#Foci	Actin Foci (mean±SD) / p-value (Mann-Whitney Test)		
			Cycle Length (s)	Duration (s)	Interval (s)
<i>sGMCA</i>	6	118	178,26 ± 60,94	85,46 ± 21,36	94,67 ± 54,65
<i>sGMCA;</i> <i>α-Cat</i> ^{I3}	5	158	185,59 ± 50,71 / 0,1471	75,95 ± 16,12 / 0,0003	109,87 ± 46,35 / 0,0029
<i>sGMCA;</i> <i>α-Cat</i> ²⁰⁴⁹	4	112	208,41 ± 56,77 / 0,0001	88,26 ± 20,13 / 0,3898	122,80 ± 46,94 / 0,0001
<i>sGMCA;</i> <i>α-Cat</i> ⁴²¹	5	86	204,65 ± 72,19 / 0,0029	71,74 ± 14,41 / 0,0001	132,91 ± 71,62 / 0,0001
<i>sGMCA;</i> <i>Shg</i> ^{g317}	4	40	238,06 ± 85,95 / 0,0001	64,87 ± 12,33 / 0,0001	173,33 ± 85,59 / 0,0001

Table S2. *Drosophila* stock list.

Genotype	Reference
<i>α-Cat</i> ¹	Sarpal et al., 2012
<i>α-Cat</i> ¹³ , FRT80E1 / TM3, Ser, Sb, GFP	This work
<i>α-Cat</i> ²⁰⁴⁹ , FRT80E1 / TM3, Sb, Ser, GFP	This work
<i>α-Cat</i> ⁴²¹ , FRT80E1 / TM3, Sb, Ser, GFP	This work
y, w, hs-Flp1.22; ; ubi-GFP, FRT80E1 / TM6B	This work
DE-Cadherin::GFP	Huang et al., 2009
DE-Cadherin::Tomato	Huang et al., 2009
DE-Cadherin::GFP; <i>α-Cat</i> ¹³ /TM3, Sb GFP	This work
DE-Cadherin::GFP; <i>α-Cat</i> ²⁰⁴⁹ /TM3, Sb GFP	This work
DE-Cadherin::GFP; <i>α-Cat</i> ⁴²¹ /TM3, Sb GFP	This work
ubi-DE-Cadherin::GFP	Oda and Tsukita, 2001
ubi-DE-Cadherin::GFP; <i>α-Cat</i> ¹ /TM6, Tb	This work
ubi-DE-Cadherin::GFP; <i>α-Cat</i> ²⁰⁴⁹ /TM6, Tb	This work
<i>α-Cat</i> ^{CP11002342}	Lowe et al., 2014
sGMCA	Kiehart et al., 2000
sGMCA; <i>α-Cat</i> ¹³ /TM3, Sb GFP	This work
sGMCA; <i>α-Cat</i> ²⁰⁴⁹ /TM3, Sb GFP	This work
sGMCA; <i>α-Cat</i> ⁴²¹ /TM3, Sb GFP	This work
<i>shg</i> ^{g317}	Tepass et al., 1996
sGMCA; <i>shg</i> ^{g317}	This work
ΔVinc	Klapholz et al., 2015
ΔVinc; <i>α-Cat</i> ¹ /TM6, Tb	This work
ΔVinc; <i>α-Cat</i> ¹³ /TM6, Tb	This work
ΔVinc; <i>α-Cat</i> ²⁰⁴⁹ /TM6, Tb	This work
ΔVinc; <i>α-Cat</i> ⁴²¹ /TM6, Tb	This work
c381-GAL4	Manseau et al., 1997
c381-GAL4, DE-Cadherin::GFP	This work
c381-GAL4, DE-Cadherin::Tomato	This work
UAS-sqh ^{DD} /CyO	Mitonaka et al., 2007
UAS-sqh ^{DD} /CyO; <i>α-Cat</i> ¹ /TM6, Tb	This work
UAS-sqh ^{DD} /CyO; <i>α-Cat</i> ¹³ /TM6, Tb	This work
UAS-sqh ^{DD} /CyO; <i>α-Cat</i> ²⁰⁴⁹ /TM6, Tb	This work
UAS-sqh ^{DD} /CyO; <i>α-Cat</i> ⁴²¹ /TM6, Tb	This work
UAS-ctMLCK/CyO	Kim et al., 2002
UAS-MbsN300	Lee and Treisman, 2004
UAS-Vinculin::Venus	This work
Vinc::GFP	Klapholz et al., 2015
Vinc::GFP; c381-GAL4, DE-Cadherin::mTomato	This work
Vinc::GFP; UAS-ctMLCK/CyO	This work
Vinc::GFP; <i>α-Cat</i> ²⁰⁴⁹ /TM3, Sb GFP	This work
Vinc::GFP; <i>α-Cat</i> ⁴²¹ /TM3, Sb GFP	This work